Environmental Research 216 (2023) 114525

Contents lists available at ScienceDirect

Environmental Research

journal homepage: www.elsevier.com/locate/envres

Ionic liquid [bmim] [TFSI] templated Na-X zeolite for the adsorption of (Cd^{2+}, Zn^{2+}), and dyes (AR, R6)

Anjani RK. Gollakota [a,**], Venkata Subbaiah Munagapati [b], Sheng-Wei Liao [a], Chi-Min Shu [a,***], Krushna Prasad Shadangi [c], Prakash K. Sarangi [c,*], Jet-Chau Wen [a,b]

[a] Department of Safety, Health, and Environmental Engineering, National Yunlin University of Science and Technology, Douliou City, Yunlin, 64002, Taiwan
[b] Research Centre for Soil & Water Resources and Natural Disaster Prevention (SWAN), National Yunlin University of Science & Technology, Douliou, 64002, Taiwan, ROC
[c] College of Agriculture, Central Agricultural University, Imphal, Manipur, 795004, India

ARTICLE INFO

Keywords:
Ionic liquids
Na-X zeolite
IFZ
Adsorption
Metals
Dyes

ABSTRACT

1-butyl-3-methylimidazolium bis(triflouromethylsufonyl)imide functionalization to Na-X zeolite (IFZ) is the primary goal of this study in order to evaluate its ability to remove heavy metals (Cd^{2+}), (Zn^{2+}), dyes Rhodamine 6G (R6), and Alizarin Red S (AR) from aqueous streams. IFZ was thoroughly examined using analytical techniques XRD, BET, FE-SEM, and FTIR, to better understand its physical and chemical properties. The surface area and the volume of pores (IFZ; 19.93 m^2/g, 0.0544 cm^3/g) were reduced in comparison to the parent zeolite (Na-X; 63.92 m^2/g, 0.0884 cm^3/g). According to SEM, the crystal structure of the zeolite (Na-X) has not been significantly altered by XRD analysis. The mechanism, kinetics, isotherms, and thermodynamic properties of adsorption were all studied using batch adsorption experiments under various operating conditions. IFZ adsorbs dyes (AR; 76.33 mg/g, R6; 65.85 mg/g) better than metal ions (Cd^{2+}; 30.68 mg/g, Zn^{2+}; 41.53 mg/g) in acidic conditions. The Langmuir isotherm and pseudo-second order models were found to be the most accurate models for equilibrium data. Adsorption is endothermic and spontaneous, as revealed by the thermodynamics of the process. The IFZ can be used in three (Cd^{2+}), two (Zn^{2+}), four (AR), and five (R6) cycles of desorption and regeneration. For these reasons, IL-modified zeolite can be used to remove multiple types of pollutants from water in one simple step.

1. Introduction

Water is a vital component of climate adaptation, as it is required for the maintenance of healthy ecosystems, the production of food and energy, and the maintenance of life itself. In addition, it has been an indispensable link between human living in the environment and the core of sustainable socioeconomic development (Gollakota et al., 2021). Hence, there must be a balance between water quality and quantity, which is important for industrial, agricultural, and domestic uses. Unfortunately, the blue planet has experienced water scarcity in recent years, which has been aggravated by water contamination from every imaginable source. Primarily, unregulated human activities, such as enormous discharges of polluted streams from transportation and industry, have serious effects on water quality (Gollakota et al., 2019). Focusing on industrial discharge streams with higher concentrations of hazardous metal traces, toxic synthetic dyes, etc., were seen as the principal dangers to aquatic ecosystems. Particularly, heavy metals (HM) such as Cd and Zn, as well as toxic synthetic dyes (SD) such as Alizarin Red S (AR) and Rhodamine 6G (R6), are detrimental to human and aquatic life because to their non-biodegradability, bioaccumulation, and bio magnification at even low doses (Mohan and Gandhimathi, 2009). Notably, Cd (II) and Zn (II) ions, which are among the most carcinogenic heavy metals, tend to disrupt the nervous system. Moreover, these HMs cannot be biodegraded and have soil residence periods of hundreds of years; they accumulate in organisms. Similarly, SDs have carcinogenic effects on human health and disrupt the aquatic photosynthetic ecology. Finally, the soil contaminated with SDs and HMs has degraded and is no longer suitable for agricultural activities due to the

* Corresponding author.
** Corresponding author
*** Corresponding author.
E-mail addresses: shucm@yuntech.edu.tw (C.-M. Shu), sarangi77@yahoo.co.in (P.K. Sarangi).

https://doi.org/10.1016/j.envres.2022.114525
Received 15 August 2022; Received in revised form 29 September 2022; Accepted 5 October 2022
Available online 13 October 2022

possibility of food chain poisoning (Visa and Chelaru, 2014). As a result, many technologies exist to remove metal ions and dye molecules from aqueous streams, such as chemical precipitation, ion exchange, adsorption, membrane separation, and so on, among which adsorption suits better due to low cost and easy operand.

On the other hand, the selection of an appropriate adsorbent material that fits the grove of economic viability and availability, is a complex challenge. Because natural materials are limited in availability, the search for alternatives resulted in zeolite materials derived from coal fly ash (CFA) being prominent (Shigemoto et al., 1993). CFA's drawback included rising energy demands, excessive coal consumption, resulting in massive combustion residues, handling, and storage difficulties (Yao et al., 2015). Whereas, the presence of Si, Al as zeolite precursors, and thermal stability still boosts the utility in water remediation, catalysis etc.

In addition to their usage as an extraction medium, ionic liquids contribute considerably to separation sciences; they can aid adsorbents increase separation performance by disaggregating nano-materials into smaller bundles. (Lv et al., 2014). Furthermore, ILs have enthralling properties such as low vapor pressure, non-volatility, flammability, a wide range of electrochemical properties, and high ion conductivity (Keskin et al., 2007). The unique molecular structure of ILs with imidazolium cations made it a promising anionic dye adsorbent material. On the other hand, nitrogen with a single pair of electrons is believed to be one of the most effective functional groups for eliminating heavy metal ions. (Joseph et al., 2020). Similar studies were reported targeting the gas separation especially CO_2 (Ilyas et al., 2018), (Kurnia et al., 2019), (Ntais et al., 2010), (Nokhodiyan Isfahani et al., 2020), and reported higher yields. However very few studies reported the synthesis of composites (IL functionalized CFA zeolites) and their utility towards the separation of metals ions and dye molecules.

Hence, the present research aims at synthesizing CFA zeolite and functionalizing with IL possessing unique adsorption phenomenon towards both metals and dye separation and altering the chemical properties upon cross-linking/grafting each other. Each of these (CFA, IL) were regarded as a significant sorbent material for dyes and metals. However, combining these compounds in optimal proportions results in a novel adsorbent that can separate both metal and dye particles from aqueous streams at the same time. Adsorption may be enhanced as a result of chemical modification of CFA by IL, which further imparts functional groups such as amines, carboxylate, hydroxyl, phosphate ions, and so on. Given the high potential of CFA-IL zeolite in dye, heavy metal ion adsorption, and reusability, this study provided a fresh look at the design of multifunctional sorbent materials.

2. Experimental section

2.1. Materials

The prime feedstock raw coal fly ash was obtained from Taichung power plant, Taichung, Taiwan; the other important materials include ionic liquid, 1-Butyl-3-methylimidazolium bis [(trifluoromethyl)sulfonyl] imide for the functionalization onto CFA zeolite was procured from Sigma-Aldrich, Taiwan (purity). Lastly, the metals Cadmium nitrate Cd $(NO_3)_2$, zinc nitrate hexahydrate ($Zn(NO_3)_2.6H_2O$), synthetic dyes Alizarin red S, Rhodamine 6G, eluents namely NaOH, H_2SO_4, HCl, HNO_3, C_2H_5OH of analytical grade were obtained from Sigma-Aldrich, Taiwan.

2.2. Synthesis of zeolite from CFA

Prior to synthesis, CFA was sieved to a finer size of 75 μm, and calcined at 800 °C for 3 h in an electric furnace in order to decarbonize/eliminate traces of carbon. This was followed by a thorough washing with de-ionized water to remove any remaining impurities before drying at 80 °C for 24 h and preparing for zeolite synthesis. The detailed synthesis process of the zeolites from coal fly ash were reported in our previous work (Gollakota et al., 2021a). The zeolite synthesis was carried out at an optimal ratio of 1:1.5 (CFA: NaOH) and fused at 500 °C for 1 h, also known as alkali dissolution reaction. The alkaline reagent of choice acts as an activator, i.e., OH^- of NaOH dissolving Si^{4+}, Al^{3+} particles in CFA. To avoid unwanted secondary reactions during the hydrothermal treatment, the fusion was carried out on a Ni crucible. The fusion mixture was quickly cooled to room temperature, finely ground, and transferred to a 100 mL Erlenmeyer flask containing 20% sodium aluminate. Sodium aluminate acts as a balancing medium, adjusting the Si/Al ratio and allowing for pure phase zeolites. The slurry was mechanically stirred at 500 rpm for 24 h at room temperature to homogenize the aluminosilicate gel. The mixture was then transferred to 100 mL polytetrafluoroethylene (PTFE) bottles that were hermetically sealed to keep out outside influences. The PTFE bottles were placed in a heating oven set to 120 °C, for 24 h, followed by filtration with Whatman paper and repeated washing to neutralize the pH of homogenized silicate gel. The gel was cured for 24 h at 150 °C to improve the structural stability of the zeolite (Na-X).

2.3. Preparation of adsorbent

The CFA zeolite and IL were co-dispersed in 50 mL of dry toluene in a refluxing assembly under vacuum. For 48 h, the mixture was refluxed at 90 °C in N_2 atmosphere. Filtration was used to remove the toluene solvent, and the solid material was transferred to a rotary evaporator. The excess physisorbed IL was removed using a low-pressure rotary evaporator. The solution mixture of CFAZ and IL was stirred for 24 h at room temperature. The overall solution of CFAZ cross-linked with IL was then dropwise added to the 1 M NaOH solution (100 mL) and equilibrated between 27 and 30 °C. The newly formed CFA-IL-Z (IFZ) material was tested for its applicability in simultaneously separating metal and dye molecules.

2.4. Characterization of the adsorbent material CFA-IL-Z

Several characterization approaches were utilized to determine the physicochemical characteristics of the raw CFA, hydrothermally treated CFA, and ionic functionalized zeolite material. At first, the material phase and zeolite identification were accomplished using X-ray diffraction (XRD, Bruker Advanced-D825A) with Cu-Kα radiation under the following conditions: scanning range $2\theta = 5\text{-}60^\circ$, scanning rate of 0.02°, 40 kV and 40 mA. The N_2 adsorption-desorption isotherm analysis was also used to evaluate the textural properties, i.e., surface area. The samples were degasified for 12 h at 423 K before being analyzed in a surface pore analyzer at 77 K. (Micrometrics, ASAP 2060). Furthermore, the pore size distribution was determined using the Brunauer-Emmett-Teller (BET) and Barrett-Joyner-Halenda (BJH) methods, respectively. The Fourier transform infrared spectroscope was used to detect the change in functional groups beginning with raw CFA, the formation of zeolites, and the impingement of ionic liquid (FTIR, PerkinElmer Spectrum One). The morphology of CFA, Zeolite (Na-X), and IFZ was further detailed using an ultra-high-resolution thermal field emission scanning electron microscope (JEOS, JSM-7610F Plus) (FE-SEM). To improve the material's conductivity, the samples were coated with a layer of gold and sputtered for 120 s. Furthermore, the changes in the functional group were identified using Fourier transform infrared spectrophotometer (PerkinElmer Spectrum One) in the scanning range of 400–4000 cm^{-1} in the presence of a DTGBr detector and a KBr split beamer. Finally, the adsorption experiments were performed on a UV–Vis spectrophotometer (PerkinElmer Lambda 850) with a quartz cell of path length of 1.0 nm at wavelengths of 396 nm (Cd^{2+}), 570 nm (Zn^{2+}), 426 nm (AR), 524 nm (R6).

2.5. Adsorption experiments

Adsorption experiments were carried out separately for metal ions Cd (II), Zn (II), and dye molecules AR, R6 in order to better understand the performance of the adsorbent material, adsorption mechanism, thermodynamic analysis, kinetics, and isotherm. Various parameters were also evaluated, including initial dye concentrations ranging from 1 to 100 mg/L, the effect of temperature (298–318 K), pH (1–10), adsorption dosage (0.1–0.5 g/30 mL), agitation speed (100–500 rpm), and the effect of time (0–300 min). Adsorption studies with variable initial concentrations revealed that 50 mg/L was appropriate and was maintained throughout the current study. The pH of the solution was changed from acidic to alkaline by adding the appropriate amount of 0.1 M NaOH and 0.1 M HCl. All experiments were carried out in batch mode, with 30 mL of the solution placed in a 100 mL Erlenmeyer's flask and shaken in an orbital sieve shaker, followed by UV–vis spectrometer analysis with an appropriate color development method for metal tracing. The color development method for metal ions for UV-analysis is mentioned in the subsequent sections. Similarly, the dyes adsorption requires no further color development and hence, they are directly calibrated under the suitable wavelength in a UV–vis spectrometer. Further, the amount of the metals ions and the dye molecules adsorbed on to the surface of the IFZ were calculated using Eq. (1), and the desorption was evaluated by Eq. (2).

$$q_e = \frac{(C_i - C_e)V}{m} \tag{1}$$

$$\text{Desorption } \% = \frac{Desorption}{Adsorption} \times 100 \tag{2}$$

2.6. Color development method for UV analysis of Cd^{2+}

2.6.1. Preparation of DBHQ solution

The spectroscopic reagent dibromo-8-hydroxyquinoline (DBHQ) has been identified as a cadmium detection reagent. It works by reacting non-adsorbent DBHQ with cadmium in a slightly acidic solution (0.00015–0.00065 M H_2SO_4) to form a highly adsorbent greenish-yellow chelate product, which can then be detected directly in aqueous solution.

2.6.2. Cadmium standard solution

Fig. 1a represents the schematic of the standard preparation procedure of stock Cd solution for UV analysis. A 100 mL stock solution of divalent cadmium was made by dissolving 0.2282 mg of AR crystalline cadmium sulfate (3 Cd SO_4 $8H_2O$) in double distilled de-ionized water. Aliquots of the solution were standardized using EDTA titration and xylenol orange indicator. 0.1–1 mL of neutral aqueous DBHQ solution (ideally 1 mL of 3.310–3 M) was added to the 10 mL calibrated flask, followed by an equal amount (preferably 0.5 mL) of 0.0005 M H_2SO_4 in a ratio of 1:100 to 1:700. Afterward, 5 mL of ethanol and deionized water were added and the liquid was diluted to the mark. The absorbance at 396 nm was compared to that of a reagent blank. The cadmium level of an unknown sample was determined using a concurrently created calibration graph.

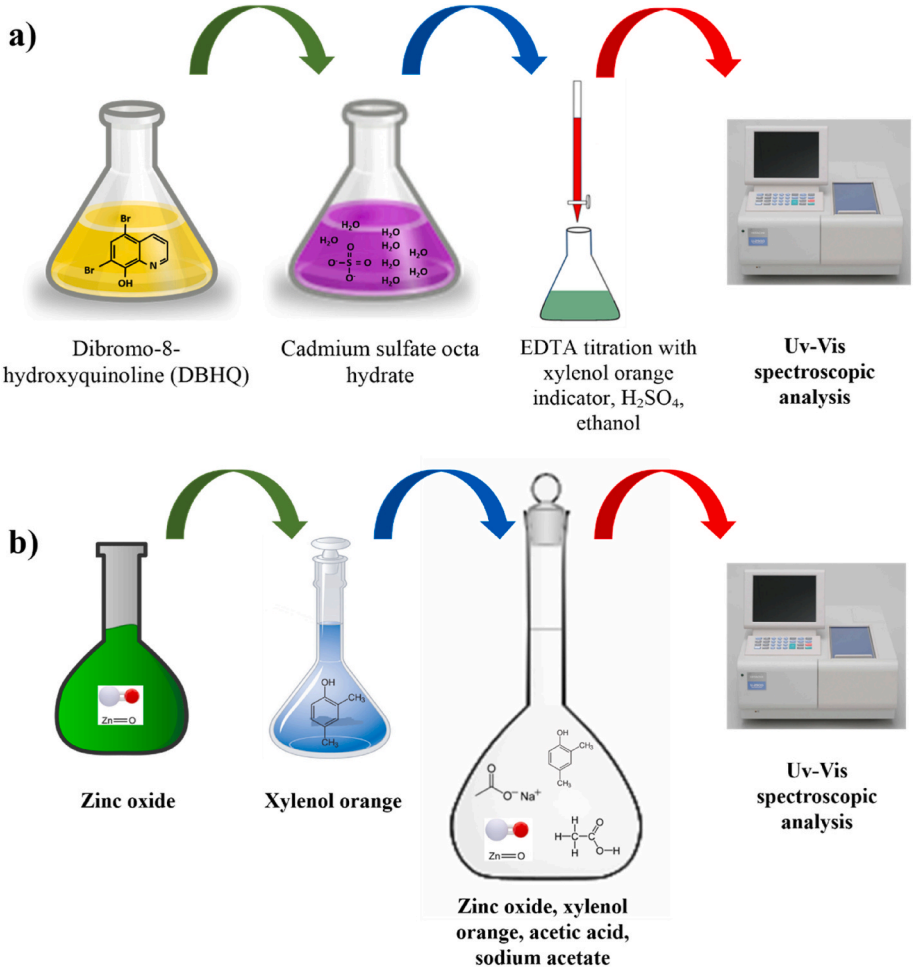

Fig. 1. a) Preparing the standard solution for UV–vis spectroscopic calibration a) Cd^{2+}; b) Zn^{2+}.

2.6.3. Zinc standard solution

The standard procedure for the preparation of Zinc solution was adopted from (Zhong et al., 2022) and (Fig. 1b). To prepare the zinc standard solution, 1.252 g of solid ZnO was placed into a 1 L volumetric flask containing 10 mL of H_2SO_4, the remaining space was filled with distilled water and the mixture was thoroughly stirred. Besides, xylenol orange solution was prepared by adding 0.15 g of xylenol orange into 100 mL volumetric flask, then add distill water to the mark on the scale and shaken vigorously. In addition, acetic acid sodium acetate buffer solution (CH_3COOH + CH_3COONa) was prepared by accurately measuring 36 mL of glacial acetic acid in a 100 mL volumetric flask, and the shaken vigorously after the addition of water. Sodium acetate (CH_3COONa) solution was prepared by adding 200 g of anhydrous sodium acetate in water followed by heating to ensure proper mixing. Further, the solution was transferred to an 1L volumetric flask containing 26 mL of glacial acetic acid (CH_3COOH), and thoroughly shaken by adding water.

2.7. Zinc ion standard curve

Standard zinc oxide solution was prepared by adding 10 mg/L of the zinc oxide into 1 L volumetric flask containing water, and the mixture was thoroughly shaken. Further, eight different standards of zinc oxide solutions (2.5 mL, 7.5 mL, 10 mL, 12.5 mL, 17.5 mL, 20 mL, 22.5 mL, and 25 mL) were prepared in 50 mL individual volumetric flasks containing 10 mL of acetic acid buffer solution and 2.5 mL of xylenol orange solution. The absorbance was measured against a standard of water using a 1 cm cuvette and a UV–vis spectrophotometer after 10 min.

2.8. Functionalization of coal fly ash-based zeolite with ionic liquids

There were three significant phases involved in the synthesis of ionic liquid immobilized on zeolite. The first step involved mixing 200 mL of Na-X zeolite with 0.002 M NH_4Cl solution for 24 h (Zendehdel et al., 2020). Filtration and washing with water were then followed by calcination at 300 °C to remove the NH_3 from the solid. In the next phase, 50 mL of dry toluene was mixed with 1 mmol of ionic liquid and refluxed for 24 h under a N_2 environment with Na-X zeolite. After filtering and drying, the solid powder was analyzed using FTIR, XRD, BET, and FE-SEM.

3. Results and discussion

3.1. X-ray diffraction

Powder X-ray diffraction (XRD) using a Philips X'Pert diffractometer (Cu-Kα radiation from a graphite monochromator) with a variable divergence slit was used to determine phase purity and crystallinity. Original CFA is mostly quartz, with tiny quantities of hematite, magnetite in the original sample, according to the XRD diffractogram. Mullite, quartz, and amorphous minerals accounted for 96% of the overall mineral composition, according to the results of a qualitative study. Due big monomineralic particles are present in a combustion process, they are often considered to be virtually non-reactive because of their high fusion temperature (Ward, 2002). The prominent "hump" in diffraction patter between 18° and 35° of 2θ shows the presence of an amorphous phase (Yang et al., 2021) (Fig. 2a). In addition, because mullite is resistant to dissolve during hydrothermal treatment, the reduced mullite percentage promotes zeolite production. Having aluminosilicate phases in all coal fly ashes studied indicated that they are suitable for the production of zeolite.

The fusion method of alkali treatment resulted in the transformation of CFA into amorphous material, with the quartz dissolved into soluble phase, which is required for the formation of zeolite. Due to the identification of pure phase zeolite template material, the ideal fusion ratio (CFA: NaOH) was chosen in this investigation. The diffraction peaks at

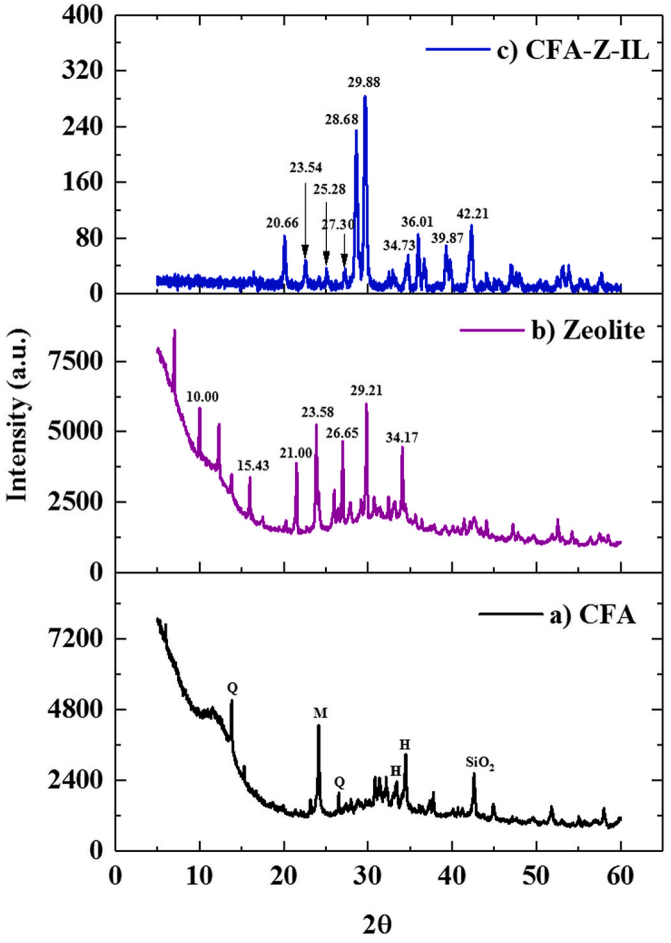

Fig. 2. XRD diffractogram of raw CFA, zeolite (Na-X), IFZ (Na-X, IL).

2θ of 15–34° which were in good agreement with the typical structure of the (FAU) topology, Further, confirmation of pure phase of Na-X belonging to the family faujisite type structure (FAU) at 2θ = 10, 15.43, 21.00, 23.58, 26.65, 29.21, and 34.17° (Treacy and Higgins, 2007) (Fig. 2b) marks the formation of a pure phase of Na-X belonging to the family of aluminosilicate molecular sieves.

And then, the XRD examination of the newly synthesized Na-X zeolite after functionalization with 1-butyl-3-methylimidazolium bis (trifluoromethylsulfonyl)imide ionic liquid was performed. The diffractogram of the composite (Na-X coupled with BMIM NTf_2) clearly displays the presence of zeolite's distinctive peaks, indicating that the functionalization technique had no effect on the zeolite host's structure (Fig. 2c). The lesser intensity bands, on the other hand, were described as indicating ionic liquid embedment on the zeolite surface. This could be explained by the disordering of the porous structure and the fluctuation in electron density caused by the ionic liquid's immobilization on the zeolite (Wang et al., 2018). Also, additional peaks at 2θ of 30–40° are attributable to the production of Si nanoparticles, intensified IFZ during the modification procedure.

3.2. Porous texture analysis

Braunauer-Emmette-Teller (N_2-BET) surface analysis technique was used to determine the surface area and pore size of the zeolite products. The N_2 as the analytical gas was employed with a Micrometrics (ASAP 2060) based on a 5 point with 30–50 desorption points. The surface area of coal fly ash prior to zeolite production was reported to be 5.15 m^2/g, while the zeolite surface area following hydrothermal treatment was reported to be 63 m^2/g, an almost 12-fold increase. Further, the (IFZ)

had a lower surface area and micropore volume than the parent zeolite (Na-X), according to BET data.

Type II is related with newly prepared zeolite (Na-X) macro porous material that falls within the classical range for BET technique application in Type II isotherm is $p/p_0 = 0.05$ to 0.3 (Deka and Bhattacharyya, 2015). This represents the unrestricted monolayer-multi layer adsorption. As shown in Fig. 3, a wide pore size distribution spanning from 1.7 to 264 nm pore diameter was detected, showing the presence of mesopores in addition to macropores. In addition, it was determined that the total surface area was 63 m^2/g and that the total pore volume was 0.0088 cm^3/g. Finally, because of the ionic liquid occupying pores, the functionalization of zeolite by ionic liquid resulted in a decrease in SBET, total pore volume, and mean pore diameter. The BET isotherm also resembles Type III with H3 hysteresis, which has the desorption shoulder and lower closure points. The H3 loop, on the other hand, is categorized as pseudo-type II since it does not reach a high plateau at high P/P0 levels (Thommes et al., 2015). This is connected to the metastability of the adsorbed multilayer due to the low degree of pore curvature and lack of stiffness in the aggregate structure (and delayed capillary condensation). Without a doubt, the IL entirely occupied the parent zeolite's pore structure, resulting in a reduction in pore size and volume reported in BET tests as 19.93 m^2/g and 0.054 cm^3/g,

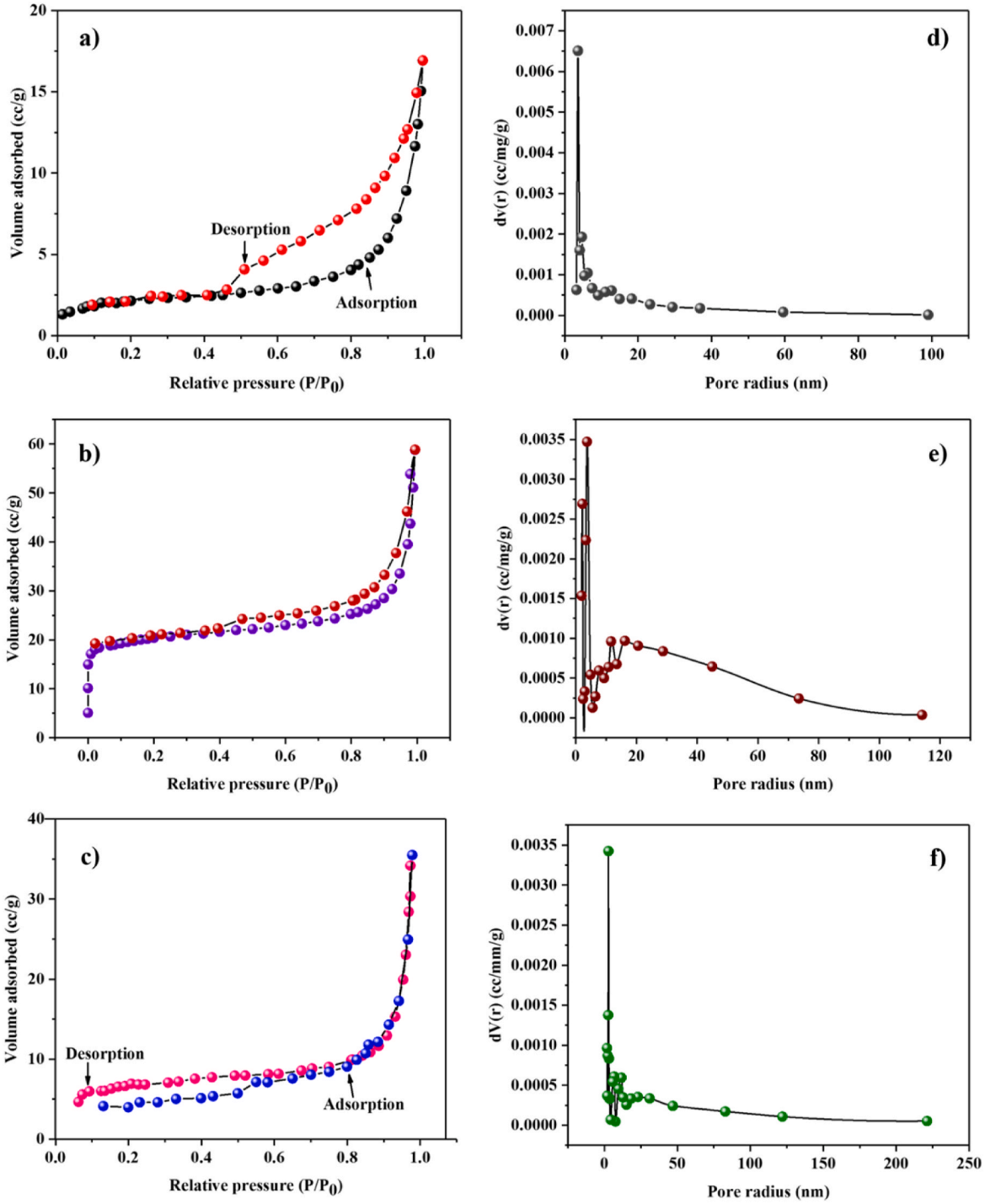

Fig. 3. Spectra of N_2 adsorption-desorption isotherm (a–c) CFA, Na-X, IFZ; BJH pore size distribution (d–f) CFA, Na-X, IFZ.

respectively. The detailed summary of the pore characteristics of CFA, NA-X, IFZ were presented in Table 1.

3.3. FT-IR analysis

FT-IR measurements were carried out on a FT-IR spectrometer (FTIR, PerkinElmer Spectrum One), in the range of 4000–400 cm^{-1} as KBr disks. FT-IR spectra reveals the mineralogical structure of the materials indicating distinct absorption patterns (Fig. 4a). A thorough knowledge on the functional group composition enables to possible adsorption mechanism of sorbate on to the sorbent surface. Fig. 4a shows the FT-IR bands of the raw CFA, zeolite (ITQ-4), ionic liquid functionalized zeolite (CFA-Z-IL).

In case of raw CFA (see Fig. 4a), the bands at 422, 485 cm^{-1} is attributed to the bending vibration of O–Si–O bonds. The bands at 453, 537, 605 is associated with Si–O vibrations, Si–O–Al bending vibrations, double stretching of Al–O respectively. The pure phase of quartz was identified at 777 cm^{-1} (Shearer et al., 2016), and the peaks at 795 (Ciocinta et al., 2012), 1058 cm^{-1} (DeCarvalho et al., 2011) indicated the symmetric and asymmetric stretching of Si–O–Si bonds. Further the peak at 798 cm^{-1} denotes the presence of quartz and its shape changes upon hydrothermal treatment indicating that the crystal structure of quartz is transformed product phase i.e., zeolite Na-X (Zong et al., 2018). An Al–O–Si/Al–O–Al band at 464 and 562 cm^{-1} is linked to the aluminosilicates in coal fly ash. While it comes to silicates in the coal fly ash, the crystalline and amorphous glassy phase were seen through the band at 1097 cm^{-1}. Si–O–Si/Al–O/Si/Al–O stretching vibration mode of AlO_6 groups of mullite causes the 506 cm^{-1} bands respectively (Yadav et al., 2021).

Further, the formation of the Na-X was examined by Fourier Transform Infrared spectroscopic techniques (Fig. 4b). The FT-IR spectra of the zeolite produced from coal fly ash is shown in Figure b. The absorption bands ascertained at 413, 432 cm^{-1} infers the bending and plane flexural vibrations of the –Si-O (DeCarvalho et al., 2011); 422, 452, 662 cm^{-1} shows the bending mode and –Si-Al-O; 467, 557, 965 represents the bending vibration of siloxane (Si–O–Si) (Zhang et al., 2021), external vibrations of double four rings (Filho et al., 2021), -Si-O asymmetric stretching vibrations (Nyale et al., 2013); and lastly 1646, 3375 cm^{-1} denotes the bending mode of physically adsorbed water and the presence of OH^- groups respectively (Hu et al., 2017). The formation of double six rings (D6R), the main structural subunit of zeolite Na-X, is indicated by the band at 561 cm^{-1}.

Lastly, the functionalization of the zeolite-X with ionic liquid were evaluated with the FT-IR analysis (Fig. 4c). The results indicated major absorption peaks at 435, 455, 496, 831, 980, 1092, 1402 cm^{-1} indicating the –Si-O-Al vibrations (El-Naggar et al., 2008), -O-Si-O bending vibrations (Zhang et al., 2019), -T-O-T symmetric bending (Gatta et al., 2015), -C-H stretching in bending plane vibration of Imidazolium iodide (Parveen et al., 2019), asymmetric stretching of Si–O–Al (Ríos Reyes, 2008), O_2^- superoxide ion vibrations, and deformed vibrations of CH_2 respectively (Ataollahi et al., 2012). In addition, the stretching of C═O and C–O and the bending of O–H at 1100-1300 cm^{-1} and 1500-1600 cm^{-1}, respectively, indicate the activation of carbon's surface by the carboxylic groups. (Kristianto et al., 2016).

3.4. Morphological analysis (FE-SEM analysis)

SEM analysis of CFA indicated a spherical morphology of fly ash, with numerous particles in the 1m size range. As illustrated in Fig. 5a, these spherical shape particles are made up of both solid and hollow spheres, as well as cenospheres. Fig. 5(b and c) shows an enlarged picture of a large particle having pores on its surface. The spherical morphology is attributed to increased Si oxides, Al-rich bituminous coals, and a glassy smooth surface due to the presence of Fe_2O_3, all of which contribute to higher pozzolanic activity and reaffirm that CFA is a good precursor for zeolite production. The morphology of the fly ash particles changes to different typical zeolite shapes during zeolitization (hydrothermal treatment of CFA) (Zeolite Na-X). The Na-X crystal has cuboid-shaped particles (Fig. 5 d-f) that are highly crystalline and come in a variety of sizes (Sumari et al., 2019). The rounded edge cuboid form of Na-X particles demonstrates that the silica and alumina species undergoing hydrothermal treatment are properly dissolving. Further, the topology of Na-X comprises a three-dimensional pore structure made up of sodalite cages similar to those found in faujisite, but coupled to the double six-membered rings (D6R) (Ríos Reyes, 2008) of $[SiO_4]^{4-}$ and $[AlO_4]^{5-}$, as validated by FT-IR analysis. Finally, the IL functionalized zeolites surface shape matches that of parent zeolites, but with a smooth layer over the top (Fig. 5 g-i). This implies that the zeolite particles have strong interfacial adhesion to the polymer matrix, indicating that the zeolite particles and the polymer are compatible. Finally, the IL functionalized zeolites (IFZ) surface shape matches that of parent zeolites, but with a smooth layer over the top. This implies that the zeolite particles have strong interfacial adhesion to the polymer matrix, indicating that the zeolite particles and the polymer are compatible. According to the results of the SEM examination, zeolite and ionic liquid grafted Na-X (IFZ) have high structural stability and can be employed as sorbent materials.

3.5. Adsorption studies

3.5.1. Adsorption as a function of pH

The pH of the solution is widely recognized to be the primary variable that drives the adsorption mechanism and determines the extraction efficiency of the selected adsorbent. The influence of pH on the adsorption of Cd^{2+}, Zn^{2+}, AR, R6 metal and dye ions on to IL functionalized Na-X zeolite was studied (Fig. 6a). The experimental results showed that the binding of Cd^{2+} is a pH dependent process-the efficiency of Cd^{2+} removal was found increasing with increasing pH from 1 to 4 to maximum value of 21.75 mg/g. Similar trends were observed for Zn^{2+}, AR, R6 dye molecules reporting the maximum uptake (27.89, 30.58, 38.29 mg/g) at pH = 5, 2, 6 respectively. Further, the electrostatic interactions between the surface charge of the IFZ and the metal ions in the solution can explain the effect of pH on adsorption capacity (Medellin-Castillo et al., 2017). At low pH values, the ability of the adsorbent to bind Cd and Zn is the weakest. This is because the metal binding sites on the adsorbent are close to H_3O^+, which makes the metal cations move away from the adsorbent. (Hashem et al., 2013). Moreover, the concentration of Cd^{2+} is almost consistent up to pH~4, after which complex tends to form namely; Cd OH^-, Cd $(OH)_2$, hydroxyl nitrate species Cd $(NO_3)_2$, $Cd(OH)_3^-$, $Cd(OH)_4^-$, $CdOH^{3+}$, and $CdNO^{3+}$ respectively (Srivastava and Angove, 2004). Similarly, at pH~6 Zn

Table 1
Morphological features of raw CFA, Zeolite Na-X, and IL functionalized Na-X zeolite (IFZ).

Sample	Si/Al	Fusion ratio (CFA: NaOH)	Fusion temperature (°C)	Sodium aluminate (%)	Crystallization temperature (°C)	BET Surface area (m^2/g)	Pore volume (cm^3/g)
CFA	3.65	–	–	–	–	5.15	0.0038
Na-X zeolite	2.12	1:1	600	20	120	63.92	0.0884
IL functionalized Na-X	–	–	–	–	–	19.93	0.0544

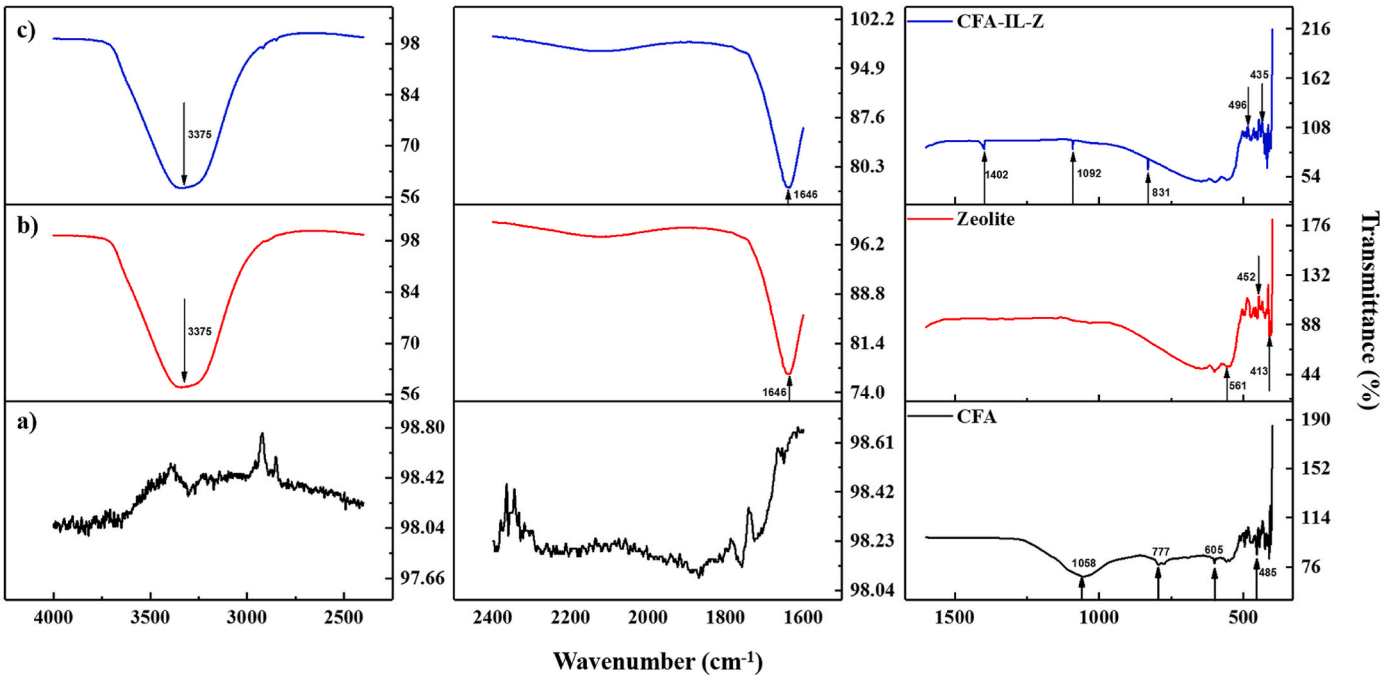

Fig. 4. FTIR spectrum of raw CFA, zeolite (Na-X), IFZ.

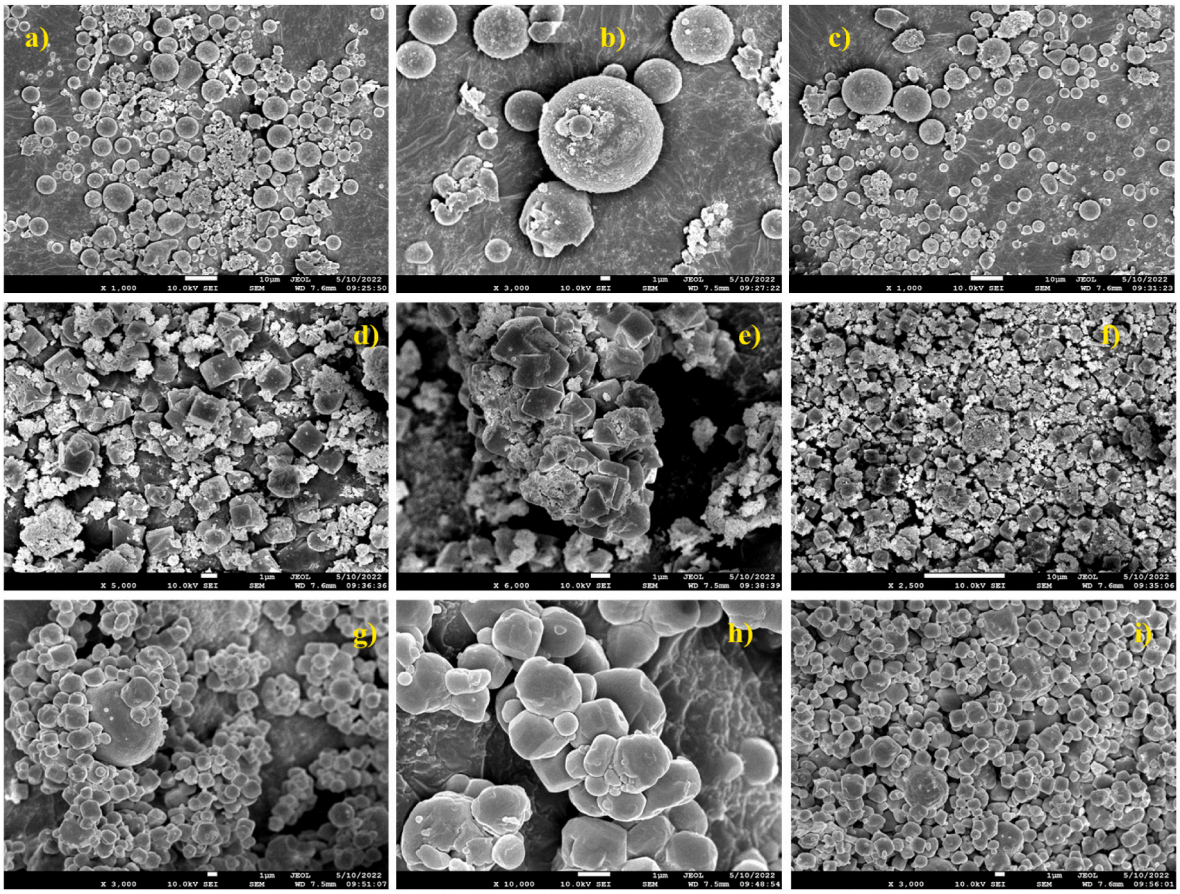

Fig. 5. SEM micrographs of raw CFA (a–c), zeolite Na-x (d–f), IFZ (g–i).

$(OH)_2$ solubility is high, and Zn^{2+} is the predominant species in the solution. In addition, as the pH increases, the solubility of Zn $(OH)_2$ decreases, and hence metal ion precipitation occurs in the alkaline range of pH (Sen and Gomez, 2011).

When it comes to dyes, acidic medium promotes protonation and neutralization of opposing surface charges, which increases mobility

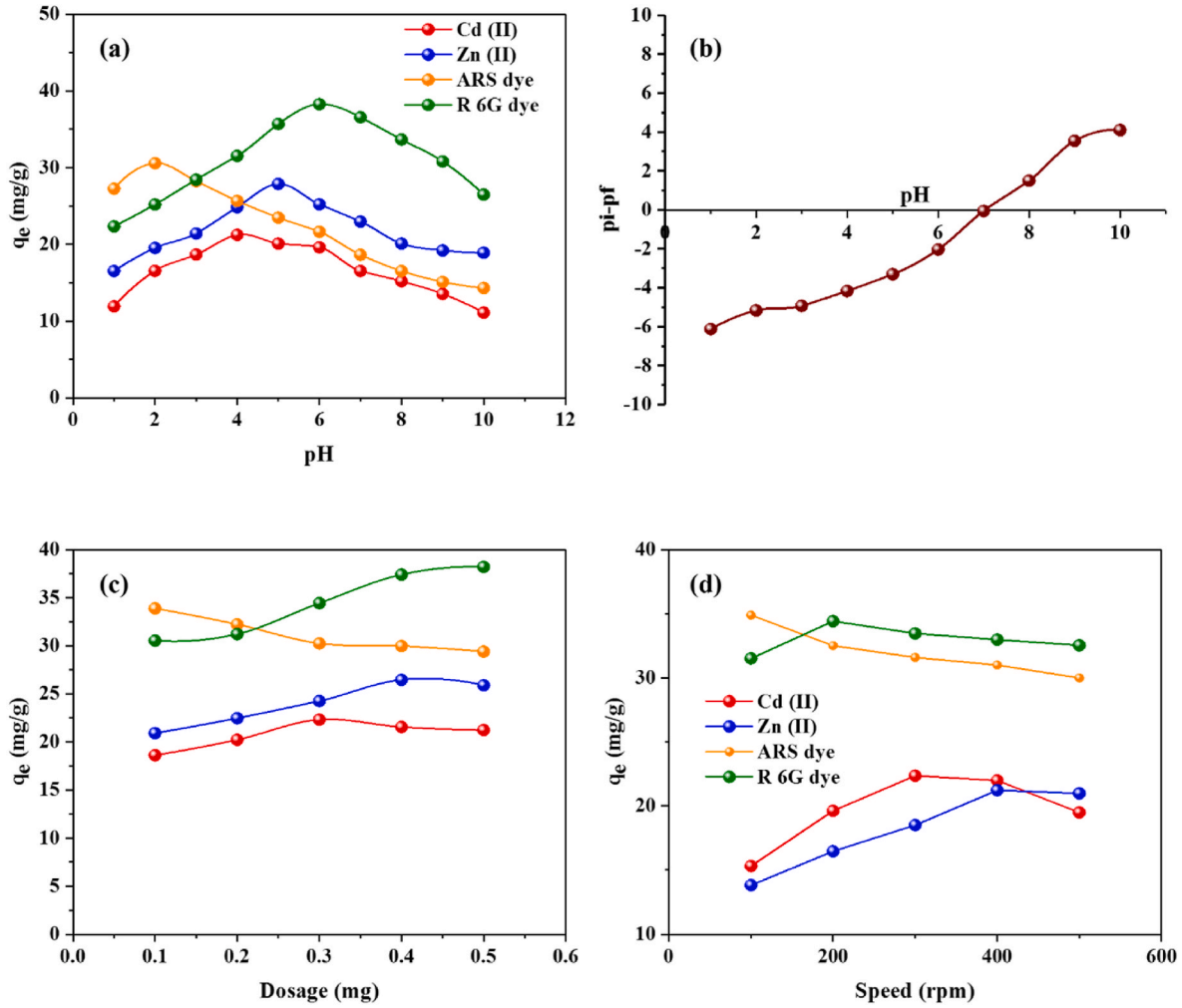

Fig. 6. Effect of process parameters on simultaneous adsorption of metals and dyes (a) pH, (b) pzc, (c) adsorbent dosage, (d) agitation speed.

towards the adsorbent and so boosts diffusion (Anjani R.K.Gollakota et al., 2021b). In contrast, retention efficiency decreased with increasing pH due to competition between protons and dye molecules for active sites on the adsorbent surface. Similarly, dye deprotonation is often possible at higher pH (alkaline medium), which prevents dye molecules from spreading across the sorbent surface (DeCarvalho Izidoro et al., 2012).

3.5.2. *Adsorption as a function of point of zero charge*

The point of zero charge (pH_{pzc}) analysis can determine the precise adsorption process and the pH confirmation. In a nutshell, the pH of the aqueous solution (0.01 M NaCl) was adjusted in the range of 1–10 with 0.1 N HCl (for pH 7) and 0.1 N NaOH (pH > 7). It is well known that at pH ≥ pH_{pzc}, cationic adsorption is dominant, whereas pH ≥ pH_{pzc}, signifies the anionic adsorption (Gomri et al., 2018). According to Fig. 6b, the selected adsorbent material's point of zero charge value was 6.9, indicating that pH ≤ pH_{pzc} is prone to anionic adsorption. The anionic binding sites in the IL functionalized zeolites mean that H^+ ions in acidic media compete with the cationic dye R6 to interact for efficient adsorption. Moreover, the present study of Cd^{2+}, Zn^{2+}, AR, R6 followed the condition of pH < pH_{pzc}, favoring the adsorption of negatively charged ions and promoting electrostatic interactions (Fig. 6b). This would imply that both SiOH, and AlOH groups are responsible of the solid's surface protonation/deprotonation reactions (Pretorius and Woolard, 2003). In summary, acidic pH favors the adsorption of both the metal ions and dye molecules towards the IFZ.

3.5.3. *Effect of adsorbent dosage*

The adsorption process's economics are totally dependent on the adsorbent dosage, which optimizes the process cost. Thus, the effect of adsorbent dosage was evaluated in treating metal ions (Cd^{2+}, Zn^{2+}) and dye molecules with five dose rates (0.1–0.5 g)/30 mL (AR, R6). According to Fig. 6c, as the dosage increases, the removal tendency of metal and dye particles behaves differently, i.e., the separation efficacy of the adsorbent towards the Cd^{2+}, Zn^{2+} was reported to be maximum 22.31, 26.45 mg/g at 0.3, 0.4 g/30 mL, and 33.89, 38.21 mg/g at 0.1, 0.5 g/30 mL for dye molecules AR, R6 respectively. At specific dosage rates, increasing surface area and unsaturated/active binding sites encourage higher sorption; beyond this, clogging/saturation of active sites, which means the increasing the diffusion path length and decreasing total adsorbent surface resulting in lesser adsorption propensity (Maleki et al., 2015).

3.5.4. *Effect of agitation speed*

The mass transfer of metal ions from the bulk liquid to the surface of the adsorbent is greatly influenced by the agitation of the liquid phase. Batch adsorption studies carried out at five different agitation speeds (100, 200, 300, 400, 500 rpm) to explore the effect of the same. As shown in Fig. 6d, the removal of metal ions reduced as the agitation speed increased, with a minor divergence for the dye molecules, showing that the uptake tendency initially increased and subsequently dropped. The maximum uptake of Cd^{2+}, Zn^{2+} was reported to be 22.35, 21.22 mg/g at 300, 400 rpm, and 34.89, 32.98 mg/g at 100, 500 rpm for AR, R6. Turbulence in the liquid phase increased the external mass

transfer coefficient, reducing the boundary layer effect and thus increasing the adsorption tendency (Garg et al., 2015). Furthermore, increasing the speed causes the sorbate to detach from the sorbent due to centrifugal forces, so the above-mentioned values were chosen to be optimal for the current study.

3.5.5. Isotherm studies

Fig. 7 depicts the amount of metal ions and dye molecules adsorbed by IFZ as a function of metal ion concentrations in solution at equilibrium. As the initial concentration of both dyes and metal ions increased, so did the amount of metal ions and dye molecules adsorbed by IFZ. Further, to evaluate this phenomenon, two popular isotherm models namely; Langmuir and Freundlich isotherms were used to study the relationship between adsorption capacity (solid phase), and concentration (liquid phase) at equilibrium. The non-linear forms of the Langmuir and Freundlich isotherms are shown in eqs. (3) and (4), and the corresponding adsorption constants reported in Table 2.

Langmuir isotherm model

$$q_e = \frac{q_m K_L C_e}{1 + K_L C_e} \quad (3)$$

Freundlich isotherm model

$$q_e = K_f C_e^{1/n} \quad (4)$$

Fig. 7 illustrates that the Langmuir equation fits the adsorption isotherms better (i.e., with higher correlation coefficients) than the Freundlich equation, with R^2 values of 0.994 (Cd^{2+}), 0.997 (Zn^{2+}), 0.998 (AR), and 0.998 (R6) at 298 K, indicating that the adsorption phenomenon favors monolayer sorption (Fig. 7 a-d) (Armbruster and Austin, 1938). In addition, Langmuir isotherm identifies a fixed number of identical binding sites, all of which are assumed to be equivalent with a homogenous adsorbent surface, and the adsorbate energies were assumed to remain constant. This means that each sorbate molecule is fitted into each vacant site of the sorbent. Moreover, the adsorption intensity measurement constant value $n > 1$ signifies the favorable conditions for adsorption (Freundlich, 1907). Besides, the full potential of the adsorbent (IFZ) was reported to be 30.68 mg/g (Cd^{2+}), 41.53 mg/g (Zn^{2+}), 76.33 mg/g (AR), 65.85 mg/g (R6) respectively at the equilibrium concentration of 50 mg/L. Likewise, other adsorption parameters values related to the Langmuir and Freundlich isotherms were presented in Table 2. Summarizing the isotherm models evaluation, the present study is highly favoring the monolayer adsorption irrespective of metal ions and the dye molecules following the Langmuir isotherm in comparison to the Freundlich isotherm fit. Lastly, the studies related to the adsorption of the selected Cd^{2+}, Zn^{2+}, AR, R6 onto the adsorbent were summarized in Table 3.

Table 2
Equilibrium modeling data for the simultaneous separation of metals and dyes.

Isotherm	Parameters	Cd^{2+}	Zn^{2+}	AR	R6
Langmuir	q_m (mg/g)	30.68	41.53	76.33	65.85
	K_L (L/mg)	0.033	0.024	0.013	0.022
	r^2	0.99	0.99	0.99	0.99
Freundlich	K_f (mg/g)	3.57	3.32	4.68	2.57
	N	2.39	2.07	1.99	1.61
	r^2	0.95	0.97	0.96	0.98

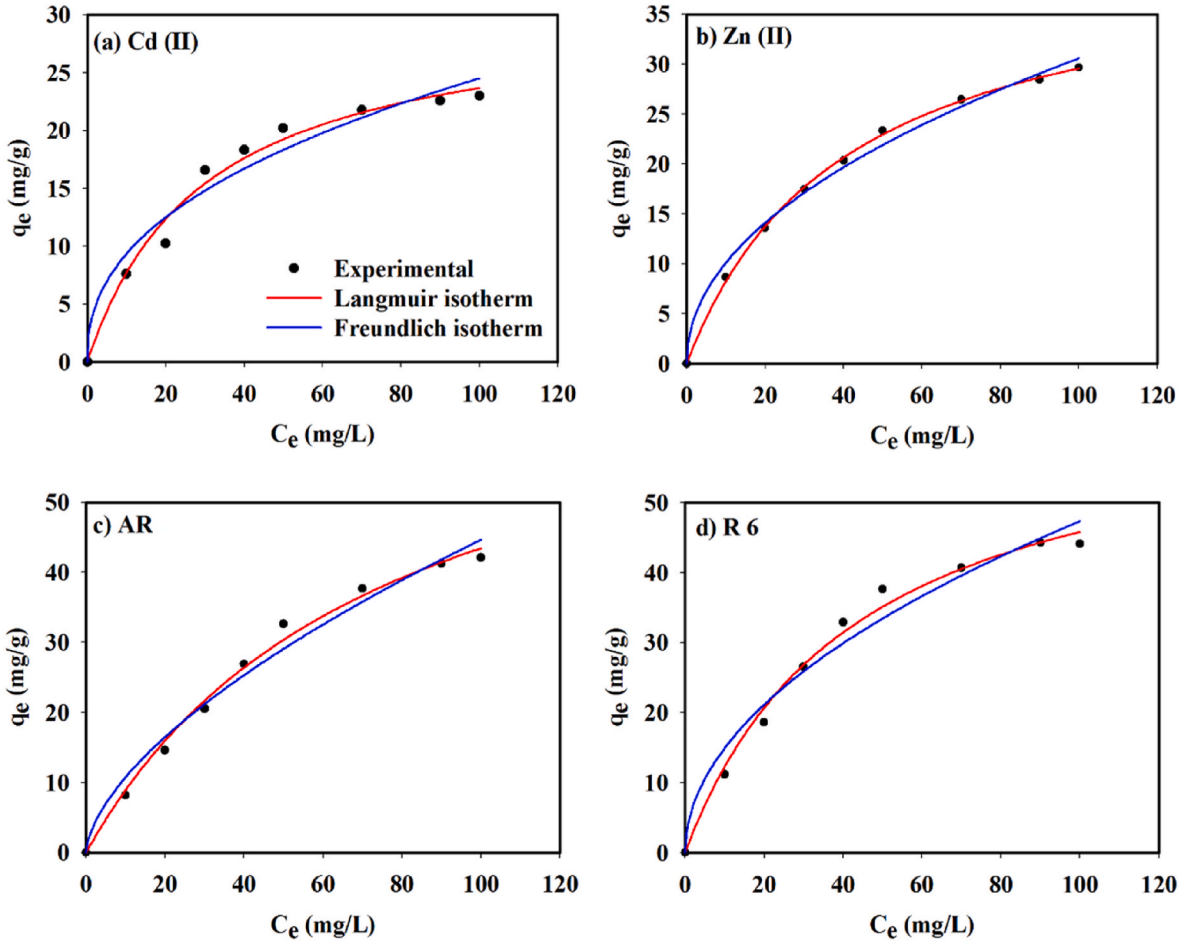

Fig. 7. Adsorption isotherm studies varied with equilibrium concentration (C_e mg/L) of metals and dyes.

Table 3
Literature on the separation of Cd^{2+}, Zn^{2+}, AR, R6 using different adsorbents.

Adsorbent	pH	Adsorption capacity (mg/g)	Reference
Cd^{2+}			
FAU-type zeolite	–	74.07	Joseph et al. (2020)
ZFA	5	17.31	Javadian et al. (2015)
Coal fly ash adsorbent	8	71%	(Mohan and Gandhimathi, 2009)
IFZ	4	30.68	Present study
Zn^{2+}			
Coal fly ash adsorbent	8	42%	(Mohan andGandhimathi, 2009)
FAU-type zeolite	–	42.017	Joseph et al. (2020)
Na-X-CS	2	83.05%	Hałas et al. (2017)
IFZ	5	41.53	Present study
AR dye			
Nano-sized Silica Modified with γ-Aminopropyltriethoxysilane Deliang	2	200	Li et al. (2011)
Multiwalled carbon nanotubes	1	161.2	Ghaedi et al. (2011)
3-aminopropyltriethoxysilane grafted silica	2	59.8	Ali et al. (2020)
IFZ	2	76.33	Present study
R6 dye			
Chitosan-g-(N-vinyl pyrrolidone)/ montmorillonite composite	10	36.66	Vanamudan et al. (2014)
hexadecyl functionalized magnetic silica nanoparticles	11	35.6	Chang et al. (2011)
Bentontie clay	6	6.233	(Farhan and Sameen, 2014)
IFZ	6	65.85	Present study

3.5.6. Adsorption kinetics

Adsorption kinetic studies emphasize the rate of solute uptake, that directly determines the adsorbate uptake residence time at the solid-solution interface. Besides, the rate limiting step is identified by kinetic models using a variety of control mechanisms such as chemical interactions, diffusion control, or mass transfer coefficients. This adsorption kinetic technique performed best when well-known pseudo-first order (Lagergren, 1989) and pseudo-second order kinetic models were used (Ho and McKay, 1999). The non-linear form of the kinetic model equations (Eqs. 5–6) listed above is as follows:

Pseudo first order

$$q_t = q_{e1}(1 - \exp(-k_1 t)) \tag{5}$$

Pseudo second order kinetics

$$q_t = \frac{q_{e2}^2 k_2 t}{1 + q_{e2} k_2 t} \tag{6}$$

In the pseudo-first order equation, the adsorbate is assigned to an adsorption site on the adsorbent, which is expressed in terms of the rate of reaction. The pseudo-second order equation suggests chemisorption involving covalent forces between adsorbent and adsorbate via electron sharing or exchange. As a result, the reaction kinetics of metal and dye uptake on the IFZ adsorbent material were studied in terms of time as a function of temperature using both the pseudo-first order and pseudo-second order kinetic models. Table 4 provides a complete description of the experimental results compared to the modeling kinetic data of Cd^{2+}, Zn^{2+}, AR, and R6 attraction to the IFZ. Fig. 8(a–l) also displays a comparison kinetic analysis with experimental observations of adsorption at temperatures ranging from 298 to 318 K. The kinetics were strongly aligned to pseudo-second order, and rising temperature increased the adsorption tendency, according to the figure. The pseudo-second order model suggests a heterogeneous surface and wither a chemisorption or an ion-exchange mechanism, depending on the functional group of the adsorbent (Ankrah et al., 2022). As previously stated, the main finding of this study was that the adsorption phenomena was chemisorptive in nature because the pathway follows pseudo-second order kinetics.

3.5.7. Temperature effects and thermodynamics

Enthalpy, free energy, and entropy were measured at 298, 308, and 318 K, respectively, to determine temperature's effect on system thermodynamics. Fig. 9a shows the influence of the temperature on the uptake of the Cd^{2+}, Zn^{2+}, AR, R6 towards the IFZ. The fact that the adsorption increases as the temperature rises clearly shows that the reaction is endothermic (Zhou et al., 2015), because of the stable sites on the IFZ's surface. This in turn augments the mobility of both metal ions (Cd^{2+}, Zn^{2+}) and dye molecules (AR, R6) towards the sorbent surface, making it easier for monolayer surfaces to form (Yang et al., 2017) verified by the Langmuir isotherm model.

In order to establish whether or not the adsorption process will proceed spontaneously, considerations of energy and entropy must be made. The thermodynamic property values serve as indicators for the practical application of the adsorption process. The thermodynamic parameters Gibbs free energy (ΔG^o), enthalpy (ΔH^o), and entropy (ΔS^o) were used to examine the features of adsorption related to temperature in this study. These parameters were calculated using following eqs (7)–(9).

$$\Delta G^0 = -RT\ ln\ K_c \tag{7}$$

$$\Delta G^0 = \Delta H^0 - T\Delta S^0 \tag{8}$$

where K_c is the distribution coefficient for adsorption and is determined as:

$$K_c = \frac{C_a}{C_e} \tag{9}$$

where C_e is the equilibrium dye concentration in solution and C_a is the

Table 4
Kinetic modeling data for the separation of Cd^{2+}, Zn^{2+}, AR, R6 using IL functionalized Na-X zeolite.

Adsorbate	Temp (K)	$q_{e,\ exp}$ (mg/g)	Pseudo first order kinetics			Pseudo second order kinetics		
			$q_{e1,\ cal}$ (mg/g)	K_1 (1/min)	r^2	$q_{e2,\ cal}$ (mg/g)	K_2 (g/mg min)	r^2
Cd^{2+}	298	22.57	25.81	0.0888	0.9538	23.19	0.0050	0.9953
	308	27.64	24.18	0.0076	0.9482	27.15	0.0047	0.9981
	318	30.11	28.09	0.1000	0.9795	31.03	0.0051	0.9947
Zn^{2+}	298	25.89	27.31	0.0045	0.9613	25.43	0.0016	0.9972
	308	27.69	26.18	0.1269	0.9733	27.43	0.0085	0.9915
	318	30.58	33.51	0.0079	0.9652	30.12	0.1358	0.9956
AR dye	298	33.97	34.18	0.0051	0.9584	34.10	0.0421	0.9968
	308	36.28	39.66	0.0018	0.9658	36.01	0.0505	0.9994
	318	39.86	41.83	0.0660	0.9522	40.01	0.0022	0.9989
R6 dye	298	36.91	38.91	0.0482	0.9758	37.11	0.0054	0.9917
	308	38.76	40.51	0.0040	0.9711	37.91	0.1028	0.9903
	318	43.54	41.30	0.1166	0.9570	44.10	0.0042	0.9945

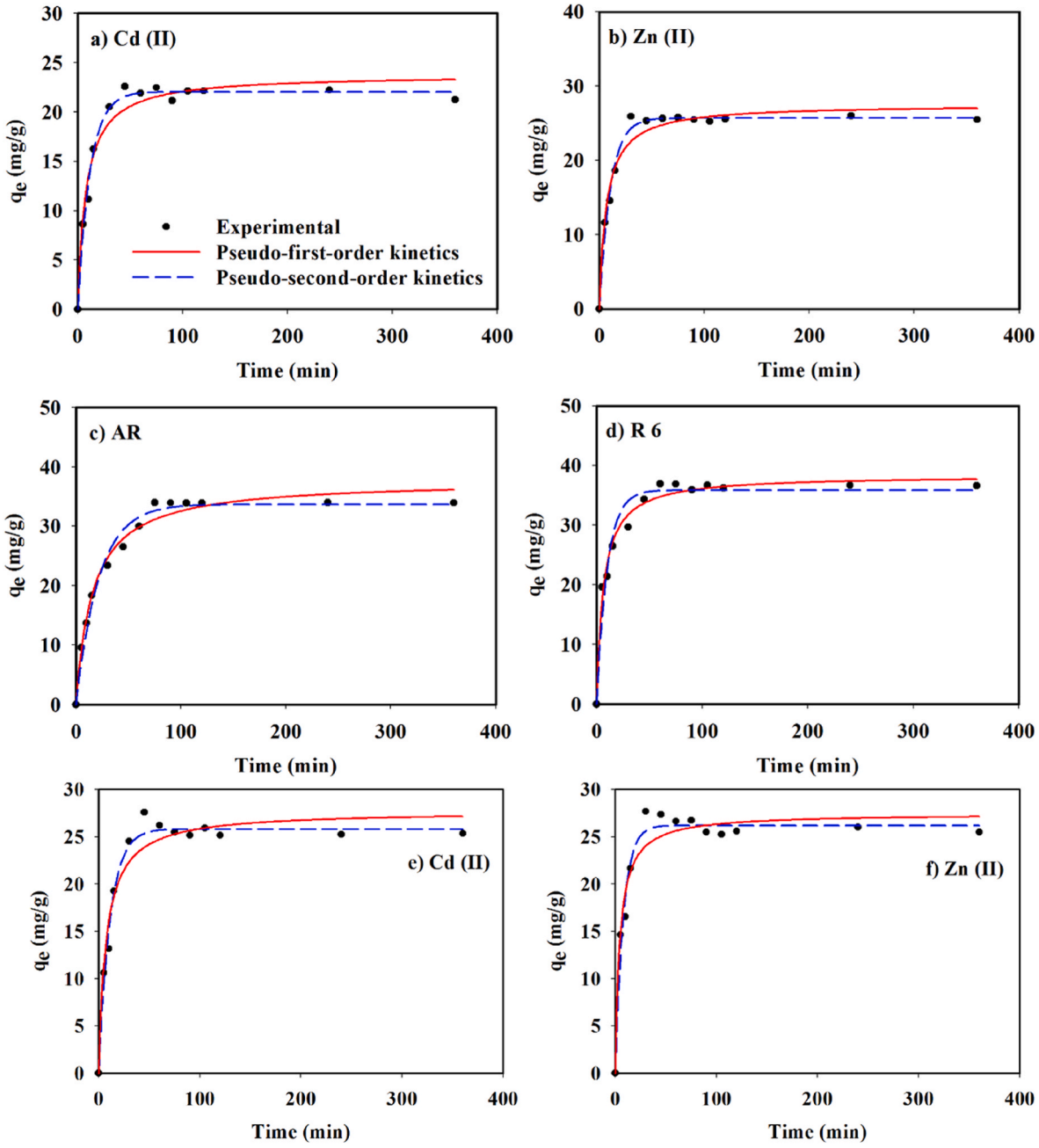

Fig. 8. Non-linear kinetic studies on the sorption of Cd^{2+}, Zn^{2+}, AR, R6 onto IFZ (a–d) 298 K, (e–h) 308 K, (i–l) 318 K.

equilibrium dye concentration on the adsorbent measured in (mg L^{-1}). Table 5 shows the Gibbs free energy (ΔG^o) for adsorption of Cd^{2+}, Zn^{2+}, AR, R6 onto IFZ at various temperatures. The slope and intercept of the ΔG^o versus T plot (Fig. 9b) were used to calculate ΔH^o and ΔS^o which are listed in Table 5. At all temperatures, the value of ΔG^o was negative, confirming the method' viability and the spontaneous nature of adsorption and suggests the attraction of the of Cd^{2+}, Zn^{2+}, AR, R6 onto IFZ at higher temperatures. The increased unpredictability at the solid-solution interface during adsorption is reflected by the positive value of ΔS^o, which indicated the IL functionalized Na-affinity X's for $Cd^{2+,}$ $Zn^{2+,}$ AR, and R6.

3.5.8. Adsorption mechanism

Electrostatic interaction, hydrogen bonding, Vander walls interaction, and ion exchange are the most common interactions between sorbate and sorbent molecules. The current study, on the other hand, is concerned with the separation of cationic metals (Cd^{2+}, Zn^{2+}), anionic dye (AR), and cationic dye (R6) using a cationic sorbent material. These metal and dye particles adsorb via electrostatic interactions for cationic and anionic subjects (Cd^{2+}, Zn^{2+}, AR, R6), and hydrogen bonding alone for anionic separations (AR) (Fig. 10). The electrostatic interactions prevail mainly due to the existence of the silanol groups (Si–OH) on IFZ. Because of the presence of silanol groups (Si–OH) on IFZ, electrostatic interactions predominate (Mesa and Becerra, 2021). Besides, the increasing sorption tendency with pH suggests that deprotonated silanol is probing greater electrostatic interactions. As a result, pH is critical in regulating the dissociation of functional groups on the active site of adsorbents. In other words, the pH values ranging between 1 and 7, favors the electrostatic interactions augmenting the enhanced uptake towards the sorbent molecule. Moreover, the hydrogen bonding is also

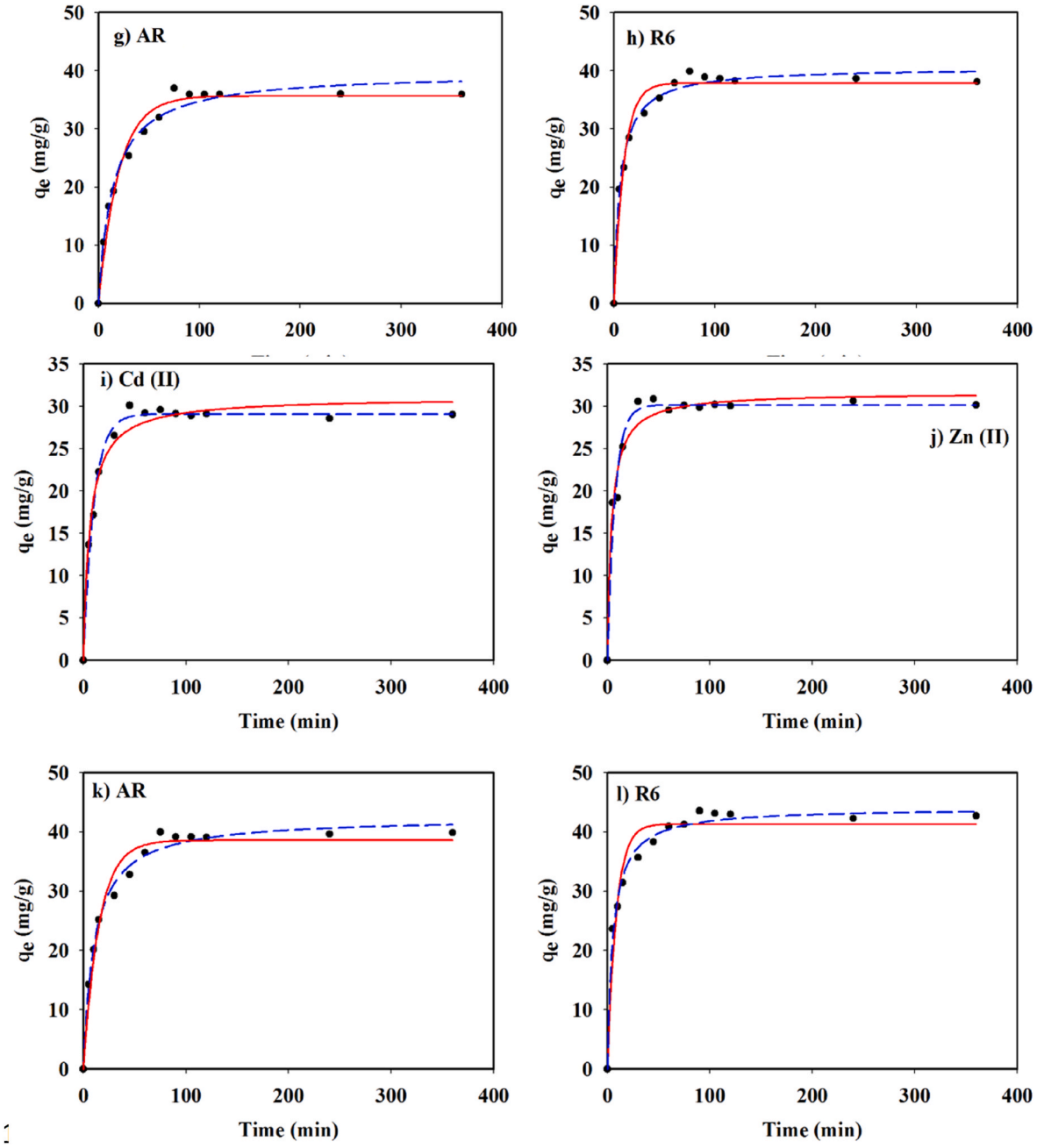

Fig. 8. (*continued*).

considered as an intermediate of covalent, ionic and Vander wall bonding (Zhang et al., 2019). This hydrogen boding makes the structure stronger, stable and provides the platform to easily disintegrate under ambient conditions. Further, the hydrogen bonding is more prevalent among the amine functional groups present in the anionic dye AR and IFZ respectively (Zendehdel et al., 2020). In summary, the predominant adsorption mechanism was electrostatic for metals, AR dye and R6 dye, additionally hydrogen bonding is possible for AR dye.

4. Desorption and regeneration studies

The desorption performance and the regeneration of the adsorbent materials were crucial to the application of sorbents in water remediation techniques. Therefore, the desorption and recycling performances of IFZ for Cd^{2+}, Zn^{2+}, AR, R6 were studied. In this desorption studies, various eluents (acidic, alkaline, alcoholic) were tested to desorb the IFZ. Among which acidic eluents solution favors the separation of adsorbent from the metal solution (Cd^{2+}, Zn^{2+}) with recovery percentage of 91, 86 respectively (Fig. 11(a and b). Similarly, the alkaline medium supporting the enhanced recovery of sorbent from the dye streams (AR, R6) of 94, and 97 percentage (Fig. 11(c and d)). The reason ascribed for the high affinity of the sorbent molecules towards the alkaline medium is due to the loosing negative ions by generation of the repulsive forces on the dye molecules forcing the detachment from the surface of the adsorbent (Sadaf et al., 2015). The suitability of the acidic eluent is highly justified in recovering sorbent from metal solutions is ascribed that; the selected acids HNO_3, H_2SO_4 contains ionizable hydrogen that could substitute the Cd^{2+}, Zn^{2+} adsorbed on IFZ (Maleki et al., 2015). Among which the ionizable hydrogen ions of HNO_3 attacks the morphological structure of IFZ than H_2SO_4, and hence HNO_3 is chosen for these assays.

Further, to evaluate the efficacy of the sorbent material, five

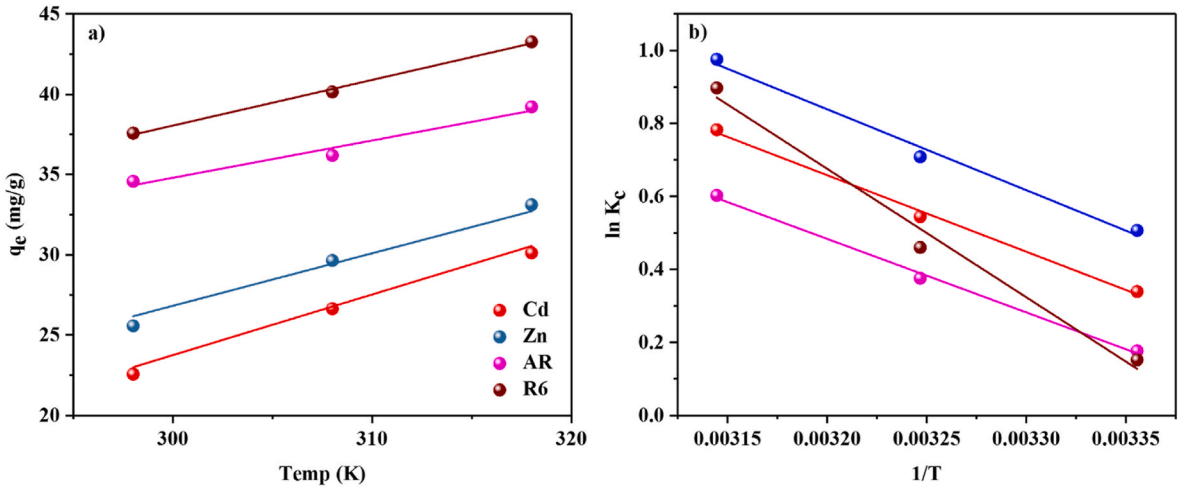

Fig. 9. Temperature effects on the adsorption of Cd^{2+}, Zn^{2+}, AR, R6 onto IFZ a) temperature effects b) Van't Hoff plot.

Table 5
Thermodynamic assessment on the adsorption of Cd2+, Zn2+, AR, R6 on to the IL functionalized Na-X zeolite.

Adsorbate	T (K)	ΔG^0 (kJ/mol)	ΔH^0 (kJ/mol)	ΔS^0 (J/mol K)
Cd^{2+}	298	−0.19821	17.6481	0.0591
	308			
	318			
Zn^{2+}	298	−1.2550	18.4312	0.0660
	308			
	318			
AR	298	−0.4371	16.7603	0.0577
	308			
	318			
R6	298	−0.3772	29.1507	0.0996
	308			
	318			

successive cycles of adsorption-desorption (regeneration) tests were performed (Fig. 12). These results suggested that the recovery of the newly prepared adsorbent material could be easily regenerated in case of the dye molecules (4 cycles for AR, R6 dye) with relatively high adsorption efficiency over the heavy metals (three cycles max for Cd, Zn) in the presence of the HNO_3, NaOH.

5. Conclusion

In the present study, ionic liquid functionalized coal fly ash zeolite (NA-X) was synthesized and successfully used for the simultaneous separation of metal ions and dye complexes. The prepared IFZ with a surface area of 19.93 m^2/g was tested for optimal time, concentration effect, adsorbent loading, concentration, agitation speed, and so on cadmium, zinc, Alizarin red S, and rhodamine 6G. Further, the structure of IFZ was not greatly affected by the IL template i.e., the present of competing ions in zeolite structure can effectively adsorb the contaminants from aqueous streams. The removal efficacy and adsorption isotherm model fitting trend were observed as R6 ≥ AR ≥ Zn^{2+} ≥ Cd^{2+}.

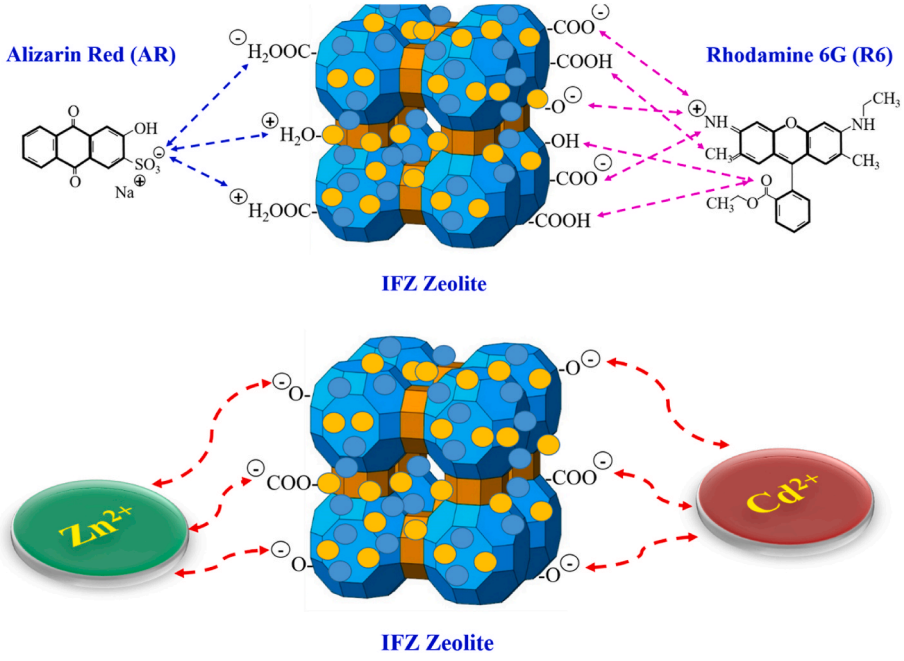

Fig. 10. Adsorption mechanism of metal ions and dye molecules onto IFZ zeolite.

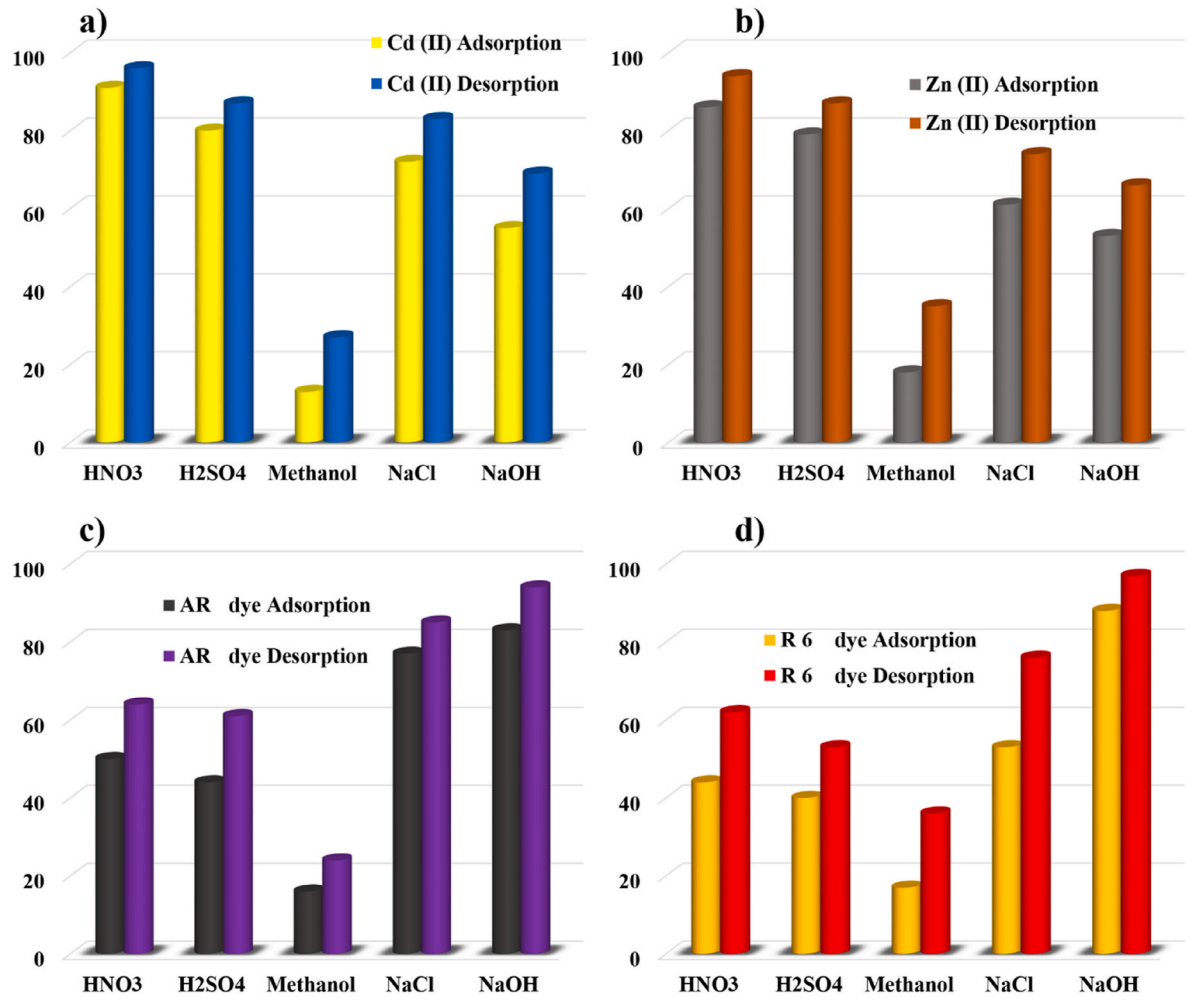

Fig. 11. Desorption studies of metal ions and dye molecules under the influence of various eluents.

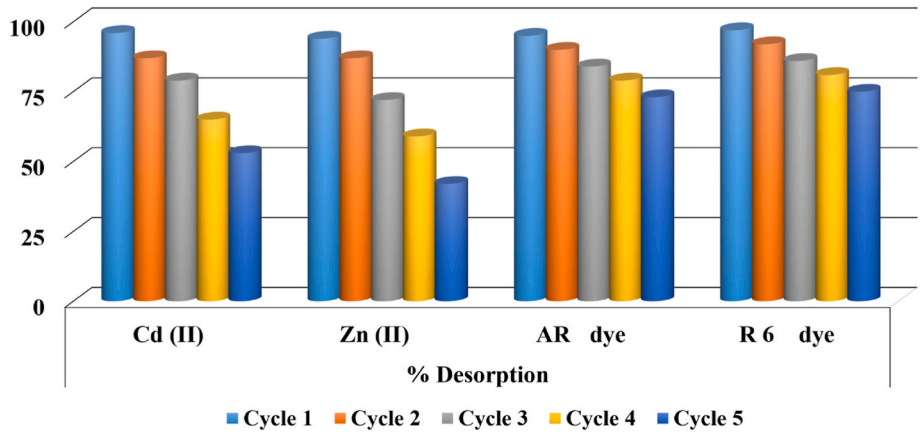

Fig. 12. Regeneration studies evaluating the ability of adsorbent for reusability.

The best fit was provided by a pseudo-second order rate equation, while the Langmuir model described the adsorption isotherm. The maximum quantity adsorbed, q_{max}, was reported to be Cd^{2+} (30.68 mg/g), Zn^{2+} (41.53 mg/g), AR (76.33 mg/g), R6 (65.85 mg/g) respectively. Lastly, the acidic medium favors the desorption of metal ions, whereas the alkaline medium favors the desorption of dye complexes. To sum up a new approach of IFZ synthesis was attempted for the potential target of introducing new single adsorbent into the database to tackle the both metals and dyes simultaneously.

Authors contribution

Anjani RK Gollakota: Experimentation, analysis, draft preparation, Munagapati V S: Experimental results validation, draft editing; Sheng-Wei Liao: Experimental analysis; Chi-Min Shu: Conceptualization, supervision and draft edition; Krushna Prasad Shadangi: revision; Prakash

K Sarangi: formating and final correction; Jet-Chau Wen: draft editing.

Declaration of competing interest

The authors declare that they have no known competing financial interests or personal relationships that could have appeared to influence the work reported in this paper.

Data availability

The data that has been used is confidential.

Acknowledgements

The authors sincerely acknowledge the cooperation of PS&DPL.

References

Ali, N., Ali, F., Ullah, I., Ali, Z., Duclaux, L., Reinert, L., Lévêque, J.M., Farooq, A., Bilal, M., Ahmad, I., 2020. Organically modified micron-sized vermiculite and silica for efficient removal of Alizarin Red S dye pollutant from aqueous solution. Environ. Technol. Innovat. 19, 101001 https://doi.org/10.1016/j.eti.2020.101001.

Ankrah, A.F., Tokay, B., Snape, C.E., 2022. Heavy metal removal from aqueous solutions using fly-ash derived zeolite NaP1. Int. J. Environ. Res. 16, 1–10. https://doi.org/10.1007/s41742-022-00395-9.

Armbruster, M.H., Austin, J.B., 1938. The adsorption of gases on plane surfaces of mica. J. Am. Chem. Soc. 60, 467–475. https://doi.org/10.1021/ja01269a066.

Ataollahi, N., Ahmad, A., Hamzah, H., Rahman, M.Y.A., Mohamed, N.S., 2012. Preparation and characterization of PVDF-HFP/MG49 based polymer blend electrolyte. Int. J. Electrochem. Sci. 7, 6693–6703.

Chang, Y.P., Ren, C.L., Yang, Q., Zhang, Z.Y., Dong, L.J., Chen, X.G., Xue, D.S., 2011. Preparation and characterization of hexadecyl functionalized magnetic silica nanoparticles and its application in Rhodamine 6G removal. Appl. Surf. Sci. 257, 8610–8616. https://doi.org/10.1016/j.apsusc.2011.05.031.

Ciocinta, R.C., Harja, M., Bucur, D., Rusu, L., Barbuta, M., Munteanu, C., 2012. Improving soil quality by adding modified ash. Environ. Eng. Manag. J. 11, 297–305. https://doi.org/10.30638/eemj.2012.038.

DeCarvalho Izidoro, J., Fungaro, D.A., Wang, S., 2012. Zeolite synthesis from Brazilian coal fly ash for removal of Zn2+ and Cd2+ from water. Adv. Mater. Res. 356–360, 1900–1908. https://doi.org/10.4028/www.scientific.net/AMR.356-360.1900.

DeCarvalho, T.E.M., Fungaro, D.A., Magdalena, C.P., Cunico, P., 2011. Adsorption of indigo carmine from aqueous solution using coal fly ash and zeolite from fly ash. J. Radioanal. Nucl. Chem. 289, 617–626. https://doi.org/10.1007/s10967-011-1125-8.

Deka, B., Bhattacharyya, K.G., 2015. Using coal fly ash as a support for Mn(II), Co(II) and Ni(II) and utilizing the materials as novel oxidation catalysts for 4-chlorophenol mineralization. J. Environ. Manag. 150, 479–488. https://doi.org/10.1016/j.jenvman.2014.12.037.

El-Naggar, M.R., El-Kamash, A.M., El-Dessouky, M.I., Ghonaim, A.K., 2008. Two-step method for preparation of NaA-X zeolite blend from fly ash for removal of cesium ions. J. Hazard Mater. 154, 963–972. https://doi.org/10.1016/j.jhazmat.2007.10.115.

Farhan, A.M., Sameen, A.S., 2014. Kinetic study of adsorption rhodamine 6G dye from aqueous solutions using bentonite clay. Am. J. Environ. Eng. 4, 11–17. https://doi.org/10.5923/j.ajee.20140401.03.

Filho, G.F., de, F.A., Araújo, A.B., de, F.S., Silva, L.R., de, B., Barros, T.R.B., Barbosa, T.S. B., Paula, G.M.de, Barbosa, T.L.A., Rodrigues, M.G.F., 2021. Valorization of solid waste (sugarcane bagasse ash) with applications in synthesis of zeolite NaA/Valorização de resíduos sólidos (cinza de bagaço de cana) com aplicações em síntese de zeólita NaA. Brazilian J. Dev. 7, 58748–58763. https://doi.org/10.34117/bjdv7n6-324.

Freundlich, V.H., 1907. Kolloidfiillung und Adsorption. Juretzka Gattierung von Zinkblende und Galmei 20, 750–754. https://doi.org/10.1002/ange.19070201806.

Garg, A., Mainrai, M., Bulasara, V.K., Barman, S., 2015. Experimental investigation on adsorption of amido black 10b dye onto zeolite synthesized from fly ash. Chem. Eng. Commun. 201, 123–130. https://doi.org/10.1080/00986445.2013.836636.

Gatta, G.D., Rotiroti, N., Bersani, D., Bellatreccia, F., Ventura, G.Della, Rizzato, S., 2015. A multi-methodological study of the (K,Ca)-variety of the zeolite merlinoite. Mineral. Mag. 79, 1755–1767. https://doi.org/10.1180/minmag.2015.079.7.03.

Ghaedi, M., Hassanzadeh, A., Kokhdan, S.N., 2011. Multiwalled carbon nanotubes as adsorbents for the kinetic and equilibrium study of the removal of alizarin red S and morin. J. Chem. Eng. Data 56, 2511–2520.

Gollakota, Anjani R.K., Munagapati, V.S., Gautam, S., Wen, J.C., Shu, C.M., 2021a. Hydrothermal tuning of morphology of aluminophosphate (AlPO-14) framework for the adsorption of Rhodamine 6G dye. Adv. Powder Technol. 32, 3002–3015. https://doi.org/10.1016/j.apt.2021.06.015.

Gollakota, Anjani R.K., Munagapati, V.S., Shadangi, K.P., Reddy, G.M., Wen, J.C., Shu, C. M., 2021b. Encapsulating toxic Rhodamine 6G dye, and Cr (VI) metal ions from liquid phase using AlPO4-5 molecular sieves. Preparation, characterization, and adsorption parameters. J. Mol. Liq. 336, 116549 https://doi.org/10.1016/j.molliq.2021.116549.

Gollakota, Anjani R.K., Subbaiah, V., Volli, V., Gautam, S., Wen, J., Shu, C., 2021. Coal bottom ash derived zeolite (SSZ-13) for the sorption of synthetic anion Alizarin Red S (ARS) dye. J. Hazard Mater. 416, 125925 https://doi.org/10.1016/j.jhazmat.2021.125925.

Gollakota, A.R.K., Volli, V., Shu, C.M., 2019. Progressive utilisation prospects of coal fly ash: a review. Sci. Total Environ. 672, 951–989. https://doi.org/10.1016/j.scitotenv.2019.03.337.

Gomri, F., Finqueneisel, G., Zimny, T., Korili, S.A., Gil, A., Boutahala, M., 2018. Adsorption of Rhodamine 6G and humic acids on composite bentonite–alginate in single and binary systems. Appl. Water Sci. 8 https://doi.org/10.1007/s13201-018-0823-6.

Hałas, P., Kołodyńska, D., Płaza, A., Gęca, M., Hubicki, Z., 2017. Modified fly ash and zeolites as an effective adsorbent for metal ions from aqueous solution. Adsorpt. Sci. Technol. 35, 519–533. https://doi.org/10.1177/0263617417700420.

Hashem, A., Adam, E., Hussein, H.A., Sanousy, M.A., Ayoub, A., 2013. Bioadsorption of Cd (II) from contaminated water on treated sawdust: adsorption mechanism and optimization. J. Water Resour. Protect. 5, 82–90. https://doi.org/10.4236/jwarp.2013.51010.

Ho, Y.S., McKay, G., 1999. Pseudo-second order model for sorption processes. Process Biochem. 34, 451–465. https://doi.org/10.1021/acs.oprd.7b00090.

Hu, T., Gao, W., Liu, X., Zhang, Y., Meng, C., 2017. Synthesis of zeolites Na-A and Na-X from tablet compressed and calcinated coal fly ash. R. Soc. Open Sci. 4 https://doi.org/10.1098/rsos.170921.

Ilyas, A., Muhammad, N., Gilani, M.A., Vankelecom, I.F.J., Khan, A.L., 2018. Effect of zeolite surface modification with ionic liquid [APTMS][Ac] on gas separation performance of mixed matrix membranes. Separ. Purif. Technol. 205, 176–183. https://doi.org/10.1016/j.seppur.2018.05.040.

Javadian, H., Ghorbani, F., Tayebi, H. allah, Asl, S.M.H., 2015. Study of the adsorption of Cd (II) from aqueous solution using zeolite-based geopolymer, synthesized from coal fly ash; kinetic, isotherm and thermodynamic studies. Arab. J. Chem. 8, 837–849. https://doi.org/10.1016/j.arabjc.2013.02.018.

Joseph, I.V., Tosheva, L., Doyle, A.M., 2020. Simultaneous removal of Cd(II), Co(II), Cu (II), Pb(II), and Zn(II) ions from aqueous solutions via adsorption on FAU-type zeolites prepared from coal fly ash. J. Environ. Chem. Eng. 8, 103895 https://doi.org/10.1016/j.jece.2020.103895.

Keskin, S., Kayrak-Talay, D., Akman, U., Hortaçsu, Ö., 2007. A review of ionic liquids towards supercritical fluid applications. J. Supercrit. Fluids 43, 150–180. https://doi.org/10.1016/j.supflu.2007.05.013.

Kristianto, H., Arie, A.A., Susanti, R.F., Halim, M., Lee, J.K., 2016. The effect of activated carbon support surface modification on characteristics of carbon nanospheres prepared by deposition precipitation of Fe-catalyst. IOP Conf. Ser. Mater. Sci. Eng. 162 https://doi.org/10.1088/1757-899X/162/1/012034.

Kurnia, K.A., Kusumawati, Y., Prasetyoko, D., Tehubijuluw, H., Alamsjah, M.A., Coutinho, J.A.P., 2019. Understanding the adsorption of ionic liquids onto zeolite ZSM-5 from aqueous solution: experimental and computational modelling. Phys. Chem. Chem. Phys. 21, 24518–24526. https://doi.org/10.1039/c9cp04717d.

Lagergren, S., 1989. Zur theorie der sogenanntan adsorption gloster stoffe. K. - Sven. Vetenskapsakademiens Handl. 24, 1–39.

Li, D., Liu, Q., Ma, S., Chang, Z., Zhang, L., 2011. Adsorption of alizarin red S onto nano-sized silica modified with γ-aminopropyltriethoxysilane. Adsorpt. Sci. Technol. 29, 289–300. https://doi.org/10.1260/0263-6174.29.3.289.

Lv, G., Li, Z., Jiang, W.T., Xu, S., Larson, T.E., 2014. Ionic liquid modification of zeolite and its removal of chromate from water. Green Chem. Lett. Rev. 7, 191–198. https://doi.org/10.1080/17518253.2014.923518.

Maleki, A., Pajootan, E., Hayati, B., 2015. Ethyl acrylate grafted chitosan for heavy metal removal from wastewater: equilibrium, kinetic and thermodynamic studies. J. Taiwan Inst. Chem. Eng. 51, 127–134. https://doi.org/10.1016/j.jtice.2015.01.004.

Medellin-Castillo, N.A., Padilla-Ortega, E., Regules-Martínez, M.C., Leyva-Ramos, R., Ocampo-Pérez, R., Carranza-Alvarez, C., 2017. Single and competitive adsorption of Cd(II) and Pb(II) ions from aqueous solutions onto industrial chili seeds (Capsicum annuum) waste. Sustain. Environ. Res. 27, 61–69. https://doi.org/10.1016/j.serj.2017.01.004.

Mesa, M., Becerra, N.Y., 2021. Silica/protein and silica/polysaccharide interactions and their contributions to the functional properties of derived hybrid wound dressing hydrogels. Int. J. Biomater. 2021 https://doi.org/10.1155/2021/6857204.

Mohan, S., Gandhimathi, R., 2009. Removal of heavy metal ions from municipal solid waste leachate using coal fly ash as an adsorbent. J. Hazard Mater. 169, 351–359. https://doi.org/10.1016/j.jhazmat.2009.03.104.

Nokhodiyan Isfahani, N., Bahadori, M., Marandi, A., Tangestaninejad, S., Moghadam, M., Mirkhani, V., Beheshti, M., Afzali, N., 2020. Ionic liquid modification of hierarchical ZSM-5 for solvent-free insertion of CO2to epoxides. Ind. Eng. Chem. Res. 59, 11970–11978. https://doi.org/10.1021/acs.iecr.0c01173.

Ntais, S., Moschovi, A., Dracopoulos, V., Nikolakis, V., 2010. Ionic liquid/zeolite composites: synthesis and characterization using vibrational spectroscopy techniques. ECS Trans. 33, 41–47. https://doi.org/10.1149/1.3484760.

Nyale, S.M., Babajide, O.O., Birch, G.D., Böke, N., Petrik, L.F., 2013. Synthesis and characterization of coal fly ash-based foamed geopolymer. Procedia Environ. Sci. 18, 722–730. https://doi.org/10.1016/j.proenv.2013.04.098.

Parveen, G., Bashir, S., Thakur, A., Saha, S.K., Banerjee, P., Kumar, A., 2019. Experimental and computational studies of imidazolium based ionic liquid 1-methyl-3-propylimidazolium iodide on mild steel corrosion in acidic solution. Mater. Res. Express 7. https://doi.org/10.1088/2053-1591/ab5c6a.

Pretorius, P.J., Woolard, C.D., 2003. The surface chemical properties of novel high surface area solids synthesized from coal fly ash. S. Afr. J. Chem. 56, 34–39.

Ríos Reyes, C.A., 2008. Synthesis of Zeolites from Geological Materials and Industrial Wastes for Potential Application in Environmental Problems. West Midlands Univ. Wolverhampt., pp. 9–21

Sadaf, S., Bhatti, H.N., Arif, M., Amin, M., Nazar, F., 2015. Adsorptive removal of direct dyes by PEI-treated peanut husk biomass: box–Behnken experimental design. Chem. Ecol. 31, 252–264. https://doi.org/10.1080/02757540.2014.950568.

Sen, T.K., Gomez, D., 2011. Adsorption of zinc (Zn^{2+}) from aqueous solution on natural bentonite. Desalination 267, 286–294. https://doi.org/10.1016/j.desal.2010.09.041.

Shearer, C.R., Provis, J.L., Bernal, S.A., Kurtis, K.E., 2016. Alkali-activation potential of biomass-coal co-fired fly ash. Cem. Concr. Compos. 73, 62–74. https://doi.org/10.1016/j.cemconcomp.2016.06.014.

Shigemoto, N., Hayashi, H., Miyaura, K., 1993. Selective formation of Na-X zeolite from coal fly ash by fusion with sodium hydroxide prior to hydrothermal reaction. J. Mater. Sci. 28, 4781–4786. https://doi.org/10.1007/BF00414272.

Srivastava, P., Angove, M., 2004. Competitive Adsorption of Cadmium (II) onto Kaolinite as Affected by pH, pp. 5–9.

Sumari, S., Fajaroh, F., Yahmin Sholihah, N., Santoso, A., Budianto, A., 2019. Effect of temperature synthesis on structural behaviours of NaY zeolite using local sand as A silica source. IOP Conf. Ser. Mater. Sci. Eng. 515 https://doi.org/10.1088/1757-899X/515/1/012036.

Thommes, M., Kaneko, K., Neimark, A.V., Olivier, J.P., Rodriguez-Reinoso, F., Rouquerol, J., Sing, K.S.W., 2015. Physisorption of gases, with special reference to the evaluation of surface area and pore size distribution (IUPAC Technical Report). Pure Appl. Chem. 87, 1051–1069. https://doi.org/10.1515/pac-2014-1117.

Treacy, M.M.J., Higgins, J.B., 2007. Collection of simulated XRD powder patterns for zeolites fifth (5th) revised edition. Collect. Simulated XRD Powder Patterns Zeolites Fifth Revis. https://doi.org/10.1016/B978-0-444-53067-7.X5470-7.

Vanamudan, A., Bandwala, K., Pamidimukkala, P., 2014. Adsorption property of Rhodamine 6G onto chitosan-g-(N-vinyl pyrrolidone)/montmorillonite composite. Int. J. Biol. Macromol. 69, 506–513. https://doi.org/10.1016/j.ijbiomac.2014.06.012.

Visa, M., Chelaru, A.M., 2014. Hydrothermally modified fly ash for heavy metals and dyes removal in advanced wastewater treatment. Appl. Surf. Sci. 303, 14–22. https://doi.org/10.1016/j.apsusc.2014.02.025.

Wang, B., Lai, H., Yue, Y., Sheng, G., Deng, Y., He, H., Guo, L., Zhao, J., Li, X., 2018. Zeolite supported ionic liquid catalysts for the hydrochlorination of acetylene. Catalysts 8, 1–13. https://doi.org/10.3390/catal8090351.

Ward, C.R., 2002. Analysis and significance of mineral matter in coal seams. Int. J. Coal Geol. 50, 135–168. https://doi.org/10.1016/S0166-5162(02)00117-9.

Yadav, V.K., Saxena, P., Lal, C., Gnanamoorthy, G., Choudhary, N., Singh, B., Tavker, N., Kalasariya, H., Kumar, P., 2021. Synthesis and characterization of mullites from silicoaluminous fly ash waste. Int. J. Appl. Nanotechnol. Res. 5, 10–25. https://doi.org/10.4018/ijanr.20200101.oa2.

Yang, J., Sun, H., Peng, T., Zeng, L., Chao, L., 2021. Study on the overall reaction pathways and structural transformations during decomposition of coal fly ash in the process of alkali-calcination. Materials 14, 1–16. https://doi.org/10.3390/ma14051163.

Yang, L., Hu, J., He, L., Tang, J., Zhou, Y., Li, J., Ding, K., 2017. One-pot synthesis of multifunctional magnetic N-doped graphene composite for SERS detection, adsorption separation and photocatalytic degradation of Rhodamine 6G. Chem. Eng. J. 327, 694–704. https://doi.org/10.1016/j.cej.2017.06.162.

Yao, Z.T., Ji, X.S., Sarker, P.K., Tang, J.H., Ge, L.Q., Xia, M.S., Xi, Y.Q., 2015. A comprehensive review on the applications of coal fly ash. Earth Sci. Rev. 141, 105–121. https://doi.org/10.1016/j.earscirev.2014.11.016.

Zendehdel, M., Khaghaninejad, S., Tavakoli, F., Ganji, S., 2020. Immobilized ionic liquid on the zeolite: its characterization and catalytic activity in the synthesis of coumarins via Pechmann reaction. J. Iran. Chem. Soc. 17, 2555–2565. https://doi.org/10.1007/s13738-020-01950-x.

Zhang, X., Du, T., Jia, H., 2021. Efficient activation of coal fly ash for silica and alumina leaches and the dependence of pb(II) removal capacity on the crystallization conditions of al-mcm-41. Int. J. Mol. Sci. 22 https://doi.org/10.3390/ijms22126540.

Zhang, Y., Wang, Z., Zhang, Z., Wu, L., Fan, Y., Sun, Z., 2019. Synthesis, characterization and adsorption behaviors of Faujasite-type zeolites towards methylene blue. IOP Conf. Ser. Mater. Sci. Eng. 592 https://doi.org/10.1088/1757-899X/592/1/012017.

Zhong, Y., An, Y., Wang, K., Zhang, W., Hu, Z., Chen, Z., Wang, S., Wang, B., Wang, Xiao, Li, X., Zhang, X., Wang, Ximing, 2022. Evaluation of aerogel spheres derived from salix psammophila in removal of heavy metal ions in aqueous solution. Forests 13. https://doi.org/10.3390/f13010061.

Zhou, Y., Min, Y., Qiao, H., Huang, Q., Wang, E., Ma, T., 2015. Improved removal of malachite green from aqueous solution using chemically modified cellulose by anhydride. Int. J. Biol. Macromol. 74, 271–277. https://doi.org/10.1016/j.ijbiomac.2014.12.020.

Zong, Y., Zhang, X., Mukiza, E., Xu, X., Li, F., 2018. Effect of fly ash on the properties of ceramics prepared from steel slag. Appl. Sci. 8 https://doi.org/10.3390/app8071187.